AN EXPERIMENTAL STUDY OF THE INTERACTIONS BETWEEN EKMAN LAYERS AND AN ANNULAR VORTEX

by

ALBERT W. GREEN, JR.

B.A., Vanderbilt University

(1960)

SUBMITTED IN PARTIAL FULFILLMENT

OF THE REQUIREMENTS FOR THE

DEGREE OF DOCTOR OF

PHILOSOPHY

at the

MASSACHUSETTS INSTITUTE OF

TECHNOLOGY

January, 1968

Signature of Author _____

Department of Meteorology, November 20, 1968

Certified by _____

Thesis Supervisor

Accepted by _____

Chairman, Departmental Committee
on Graduate STudents

Lindgren

MASS. INST. TECH.
DEC 9 1968
LIBRARIES

Acknowledgment

During this study I have been encouraged and aided by the enthusiasm and confidence of my advisor, Professor Erik Mollo-Christensen. Professors Robert Beardsley and Peter Rhines have also given constructive commentaries during the later stages, as the thesis neared completion. Fine points of the machinists art learned from Mr. E. Bean helped greatly in the construction of the apparatus.

This research has been supported by the National Science Foundation under grant GA 1439.

CONTENTS

Plates

Table

ABSTRACT

AN EXPERIMENTAL STUDY OF THE INTERACTIONS
BETWEEN EKMAN LAYERS AND AN ANNULAR VORTEX

Albert W. Green

Submitted to the Department of Meteorology on November 19, 1968
in partial fulfillment of the requirement for the degree of
Doctor of Philosophy

Transitional Ekman boundary layers (local Reynolds number > 56) are found to couple with the zonal flow in a rotating axisymmetric source-sink apparatus. The apparatus is a circular annulus with axial boundaries perpendicular to the axis of rotation. The outer (source) and inner (sink) boundaries are porous, reticulated polyurethane plastic. The working fluid is air and the velocity sensors are hot wire anemometers.

The coupling between the Ekman layers and the inviscid annular vortex which forms the core of the source-sink flow changes abruptly upon transition from laminar to non-linear state in the boundary layers. The mean response of the laminar Ekman layers to forced motion by the core oscillations is a net efflux of mass while the transitional boundary layers are non-divergent. The interactions between the annular vortex and the Ekman layers are highly coherent, and periodic in space and time as determined by electronic spectral and correlation techniques. Definite spatial structure of the three-dimensional core waves suggest that they may correspond to some of the inviscid inertial modes of the vortex.

Thesis Supervisor: Erik Mollo-Christensen
Title: Professor of Meteorology

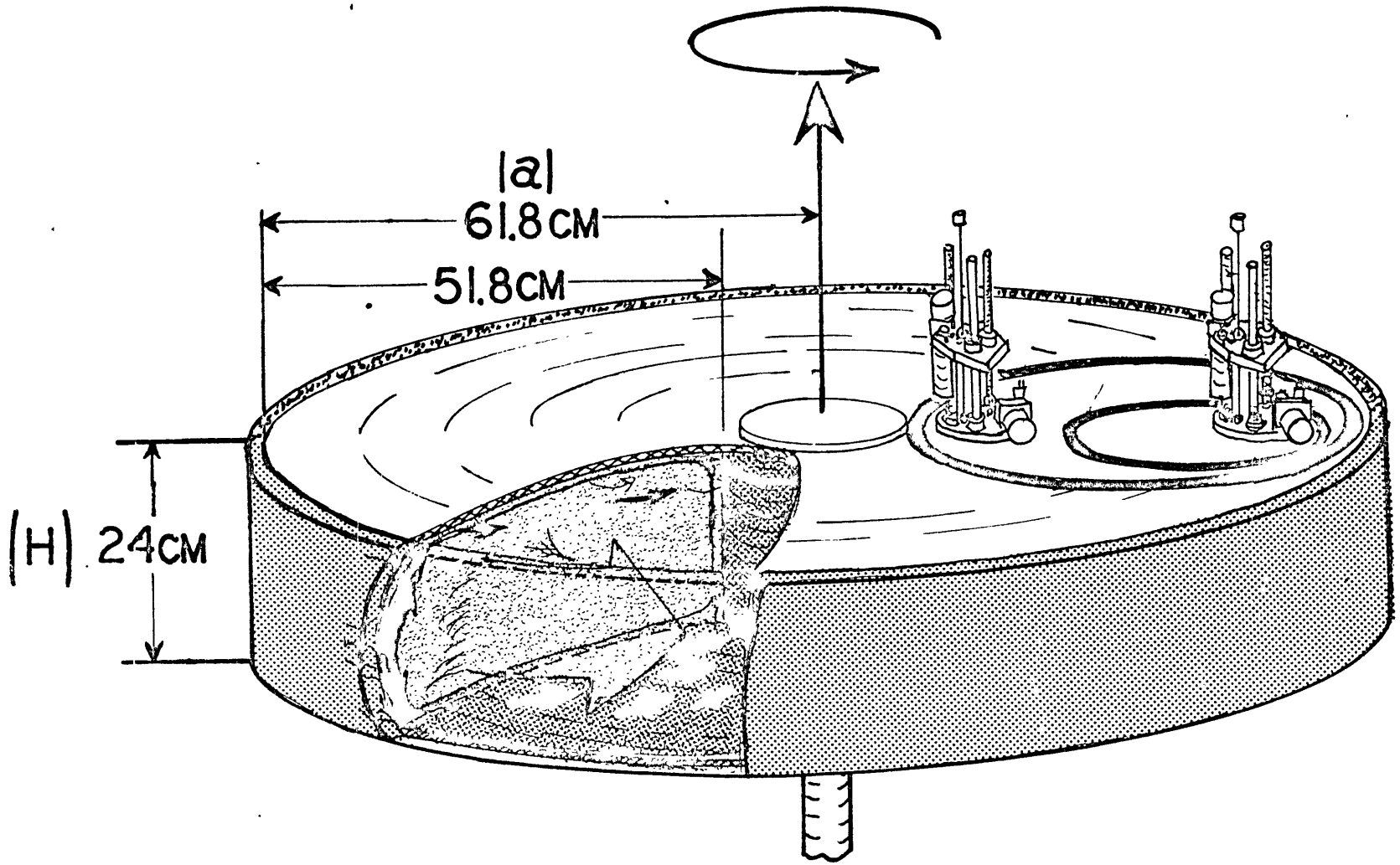

THE ROTATING ANNULUS

AIR ENTERS THROUGH THE OUTER POROUS WALL AND IS EJECTED AT THE CENTER.

FIGURE 1 A

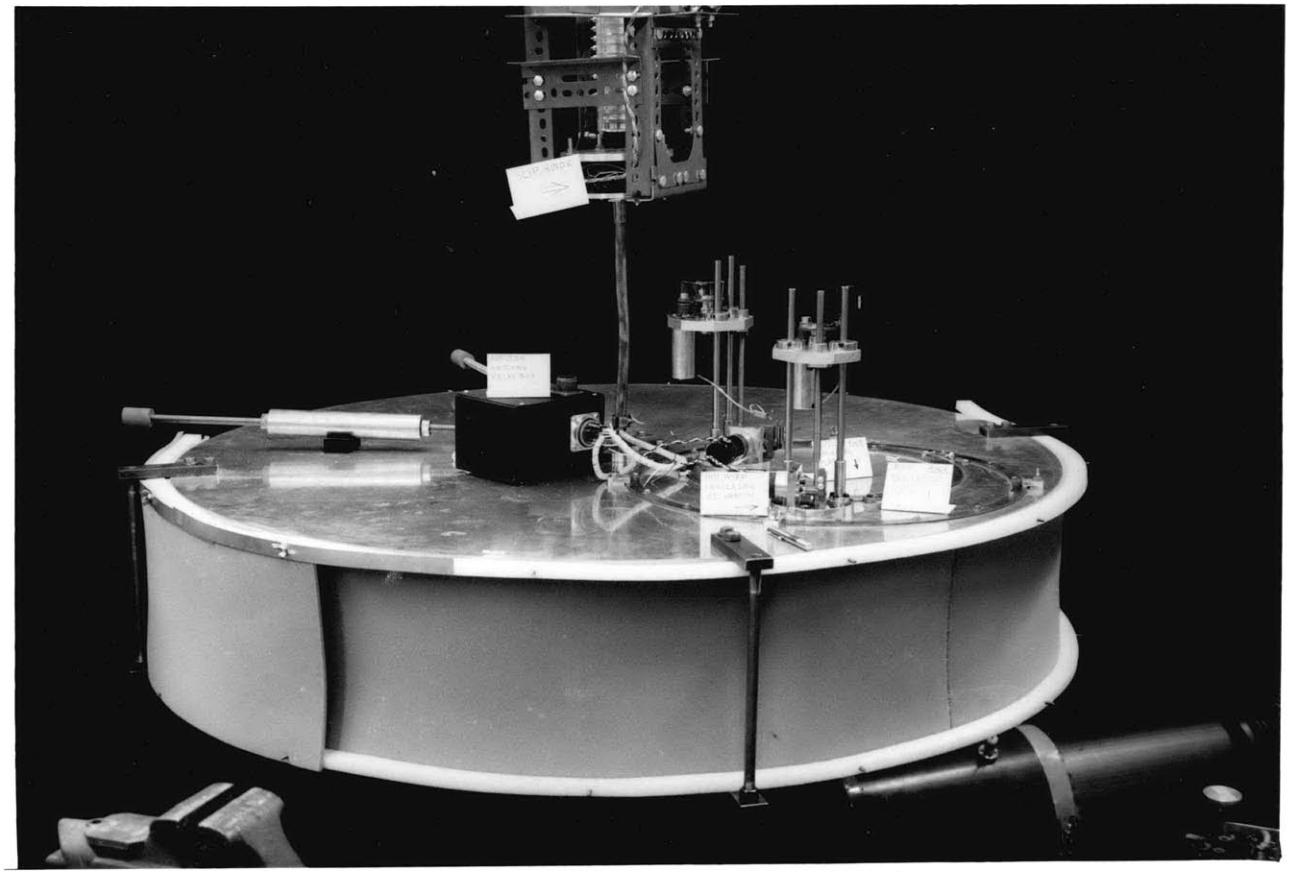

Figure 1B. Rotating annulus. Outer sheet of polyurethane foam on the source wall has been partially detached. (See appendix C for details of source configurations.)

Introduction

Tatro and Mollo-Christensen (1967) investigated the incipient instability of Ekman Boundary layers using an apparatus consisting of a hollow cylindrical annulus which was rotated about its center. (See figure 1A.) Air was drawn through the outer vertical wall into the apparatus via a porous screen and was ejected at an equal rate through the inner wall. In an axisymmetric source-sink flow, such as this, nearly all of the mass transferred radially through the apparatus is carried by the Ekman boundary layers on the horizontal surfaces. (See Faller 1963, and Hide, 1968). Tatro and Mollo-Christensen using hot wire anemometers were able to observe instabilities in the Ekman layer which occurred at two Reynolds numbers determined by the rotation and flux rates. As a by product of their investigation and later work (Mollo-Christensen, Tatro and Green, 1967), they found that oscillations occurred in the interior of the flow at the onset of Ekman layer instabilities. The present investigation describes the interior oscillations and their relationship to Ekman instabilities.

The mean flow in this system is axially symmetric and steady as long as the Ekman layers are stable, but as soon as the Ekman layer goes unsteady, oscillations occur throughout the interior. These oscillations occur in narrow range of frequencies and have definite spatial structure which could correspond to the normal modes of the columnar vortex comprising central core of the flow. The problem of the oscillations of an inviscid annular vortex is discussed in relation to the observed waves and the etastiod-inertia waves of Kelvin (1880).

2.0 The Experiment

The apparatus employed in this experiment is represented schematically in Figure 1A and is rendered photographically in Figure 1B. It can be described in a general way as a rotating, axi-symmetric, source-sink system comprised of a hollow annulus with rectangular cross-section, with the source and sink walls forming the outer and inner walls, respectively; these are both made of porous, reticulated polyurethane foam. The upper and lower horizontal surfaces are parallel polished metal disks. These disks are held apart at their centers by a hollow porous steel cylinder. This whole assembly is connected to a hollow pipe concentric with its axis, this in turn supports the apparatus and joins it to the rotation rate and flux control subsystems (Figure 4). In operation the annulus rotates on its center about the vertical axis. A small steady, negative radial pressure gradient is impressed across the annulus by the axial blower (Figure 4), causing a slow flow of air from the laboratory to enter the annulus. When the boundary layers throughout the interior are stable, mass is transfered across the annulus from source to sink via the Ekman layers which cover the horizontal surfaces. The steady axi-symmetric cases for flows of this type are discussed in detail by Lewellen (1964) and Hide (1968). If the flux through the annulus is continually increased, the equilibrium balance within the Ekman layer among the Coriolis, viscous dissipative, and pressure gradient forces breaks down and an instability results.

Mollo-Christensen and Iatro and Green(1967) had recognized the connection between onset of boundary layer instabilities and oscillations

within the core of the flow, however, limitations inherent in our apparatus prevented us from ascertaining the spatial scales of the core motions or their temporal coherency. The investigation in its next stage concentrates on the relation of these core motions to the Ekman instabiltities in the apparatus. This has required a considerable advance in technical complexity. In this experiment there are five subsystems ancilliary to the basic apparatus:

1. Sensor Position Control (Figure 2)
2. Velocity Sensors (Figure 3, center)
3. Recording and Analysis (Figure 3)
4. Flux Control (Figure 4)
5. Rotation Rate Control (Figure 4)

2.1 Position Control

The radial and azimuthal positions of the two hot wire anemometers (velocity sensors) are controlled manually by rotation of the circular inserts in the top surface of the annulus (see Figure 1A and B). The maximum angular separation allowable in this configuration is 60° at a radius of 35 cm and the range of radial separation is 5.0 to 35 cm while the maximum range of radial positon is from 11.2 to 57.6 cm with error at ± 1.5 mm. Axial positions and angular orientations of the probes with respect to the mean flow are regulated and measured by electrically powered traversing mechanisms (Figure 2) capable of continuous variation from zero to 15 cm axially with precision ± 0.004 cm. The angular orientation of the probes can be controlled within ± 1°.

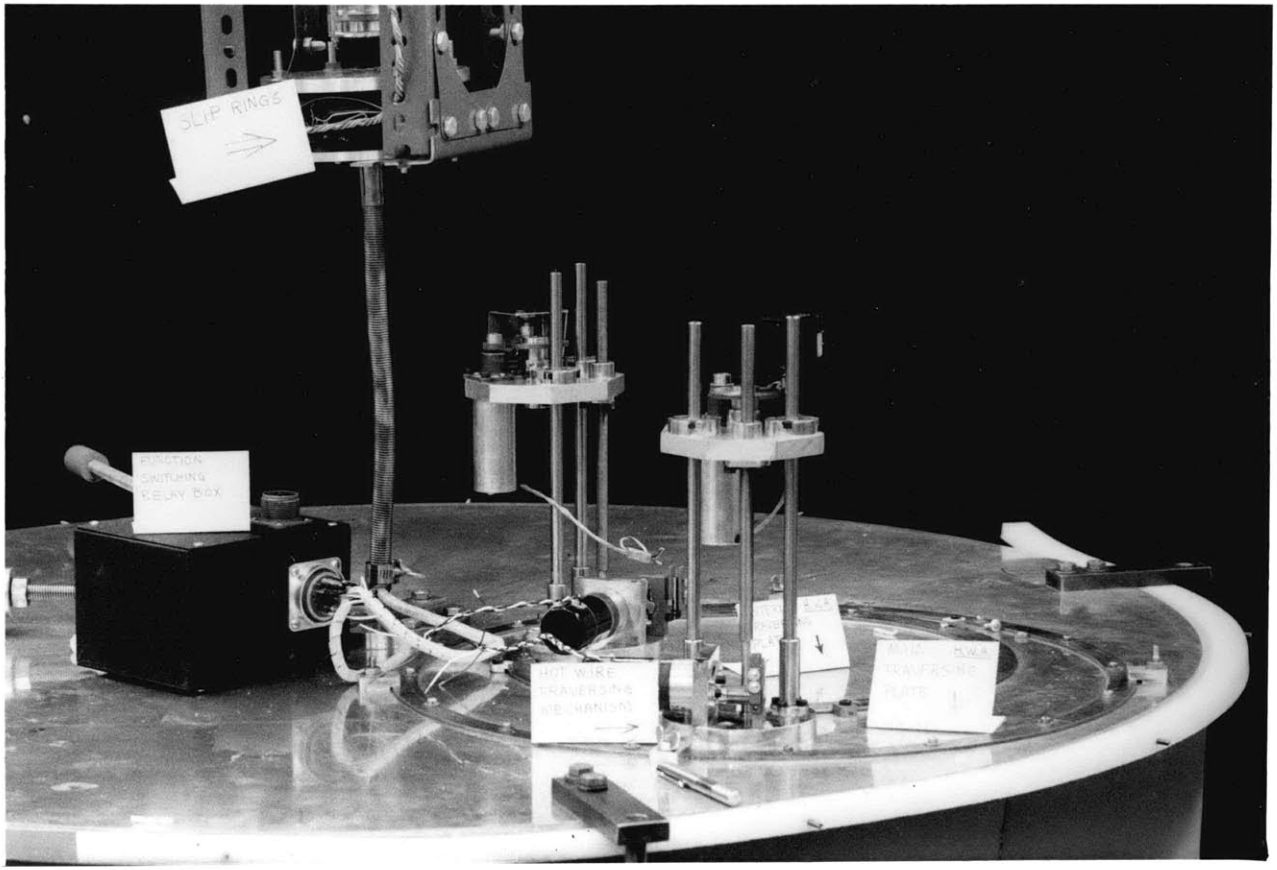

Figure 2. Velocity sensor position control.

2.2 Velocity Sensors

The velocity sensors are constant current hot wire anemometers with an x-array configuration. This subsystem includes standard battery powered current controls, bridges, galvanometers, voltage dividers and linear DC amplifiers (Figure 3). The sensors in the rotating annulus are connected to the rest frame by electrically noiseless, viscous metal sliprings. Calibration of the hot wire anemometers was performed in a small wind tunnel similar to that used by Tatro (1966). The porous-urethane foam on the source wall kept the air in the annulus virtually dust free, so that the "aging" due to contamination so common to hot wires in open systems, was virtually eliminated. Elimination of aging reduced the problems of calibration of a given wire considerably, since the only other major factor in the change of calibration values is the fluctuation of ambient temperature. The mean hot wire voltages were nullified by voltage dividers before amplification by the DC amplifiers so that velocity fluctations could be observed separately.

2.3 Recording and Analysis

The recording and analysis subsystem (Figure 3) consists of two tape recorders, a frequency spectrum analyzer, a correlation computer, and a small analog power spectrum computer. Unfortunately the power spectrum computer did not function properly so its output is only qualitative for power amplitudes over the observed spectrum. The data in the form of amplified (x1000) voltage fluctuations were recorded on two channels of the first tape recorder (Figure 3) using frequency modulation techniques to transform the signals to information which

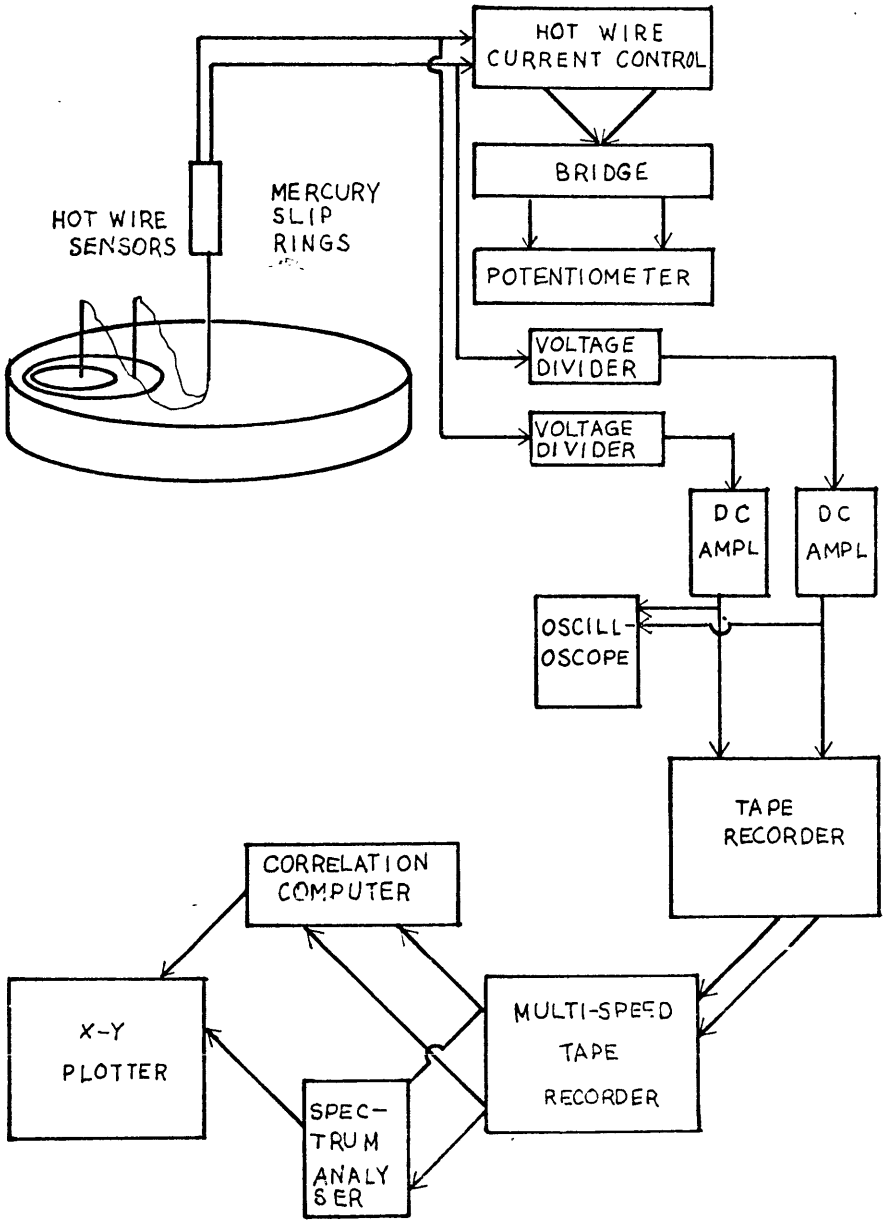

FIGURE 3

Data recording and Analysis subsystems

could be recorded on standard magnetic tape. Next the data are transfered from the first recorder to a second which records the data on a continuous tape loop capable of storing approximately two minutes of continuous data. The second tape recorder then replays the tape loop at a tape speed one hundred times greater than the original recording, the two minutes of data are then compressed in time to 1.2 seconds. This brings a block of low frequency information into a range of frequencies amenable to analysis by analog methods. From the second recorder the accelerated data signals are routed to any of several analog data analysis instruments.

When the accelerated data are transmitted to a correlation function computer, (such as the Princeton Applied Research Model 101 used here) we obtain auto correlations of two probes which are spatially separated. The root mean squares of the fluctuations are also given as the correlation at a zero time delay. The spectrum analyzer is programmed to scan a given input frequency band at a fixed rate, and its output is a voltage proportional to the amplitudes of the input signal frequencies across the band. This output signal may be plotted on the x-y recorder by using the demodulated output of the analyzer's beat frequency oscillator as the frequency coordinate and the output of the analyzer as the amplitude coordinate.

The x-y recorder is also used to record the correlation functions where the output of the correlation computer is plotted against time over the total delay time of one signal with respect to another.

2.4 Flux Control

The flux control subsystem consists of the calibrated flux meter, baffle, perforated cylindrical sleeve and its flexible cover, and an axial fan; all of which are connected together with flexible ducting as shown in Figure 4. The calibrated flux meter is a device similar to that used by Tatro and Mollo-Christensen (1967) which is basically a pipe within which is a series of flow rectifying screens, a small cylindrical bar extending across the pipe's diameter, followed by a hot wire anemometer in the wake of the bar. At low flux rates the wake of the bar becomes turbulent and forms a vortex street whose frequency is proportional to the volume flux through the pipe. Volumetric flux versus shedding frequency was calibrated over a large range using an American Meter Corporation standard proof meter. The result of this calibration showed that the shedding frequency varied linearly ± 1.5% with the volumetric flux over a range from 600 cm^3/sec to 3200 cm^3/sec. The perforated cylindrical sleeve with its flexible rubber covering provide the control of the flux, by increasing or decreasing the covered area of the sleeve which in turn increases or decreases the differential pressure provided by the fan.

2.5 Rotation Control

The rotation rate control system includes magnetic reed switching assembly, DC motor and control unit, and a preset counter. The switching assembly consists of an annular disk with five small magnets equally hollow rotating shaft in proximity to the reed switch, which closes when each magnet passes. When the switch is activated, an electrical signal is

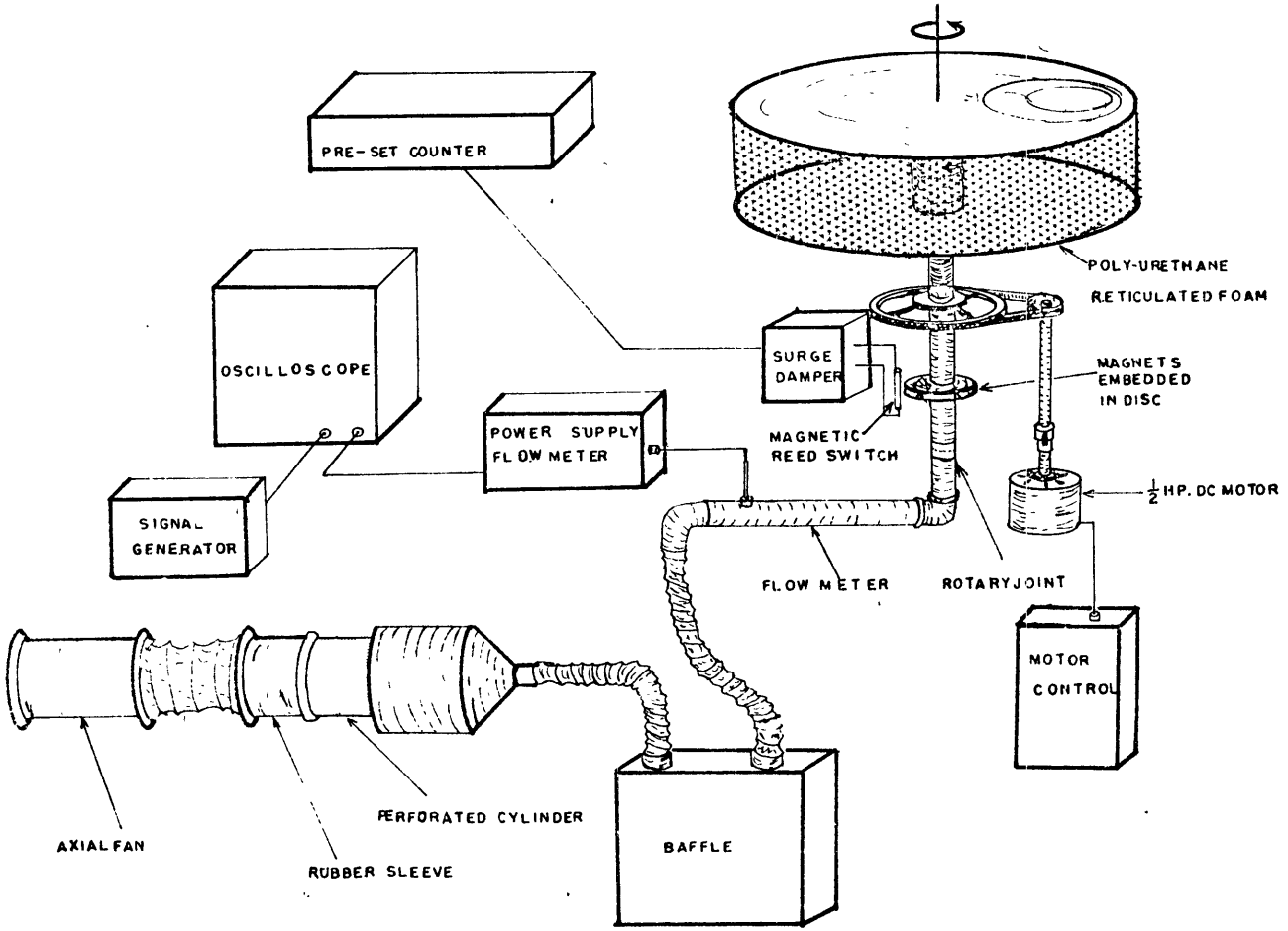

FIGURE 4 SCHEMATIC OF THE ROTATION RATE AND FLUX CONTROL SUBSYSTEMS

sent to the preset counter which indicates the period of rotation. The power for rotation of the annulus is provided by the 1/2 hp DC motor and its control unit. Once the basic rotation rate is set the deviations can be maintained at less than 1% utilizing fine torque adjustments on the control unit.

Unfortunately rotating systems with accurate control and measuring capabilities are very complex. For more complete technical information refer to Appendices A-D in the thesis.

3.0 Vibrations of an Annular Vortex

3.1 An Old Problem

More than a century ago Lord Kelvin published his commentaries, on "Vortex Atoms" (1867) in which he attempted to rectify, if not devastate, a popular theory of the constitution of matter which had gained some popularity at that time. Judging from his collected works, it appears that the intricacies of vortex motion intrigued him for a number of years. In 1880 he presented "Vibrations of a Columnar Vortex" which amounted to his final significant work on this subject. In this he solved the most tactable examples from the "crowds of interesting cases" which had appealed to him, and left the mathematically complicated cases to those who felt that such challenges were worthwhile. The cases which he presented showed that inviscid fluids in an organized state of vortex motion respond to small oscillatory perturbations. This response is simple harmonic; however the modifier "simple" in this instance is a misnomer, since the vortex oscillations are usually three dimensional inertial waves which are difficult to visualize, or observe, except in the most elementary cases. Many authors have worked Kelvin's examples, and have applied the results in various contexts; i.e. V. Bjerknes et al (1933) in geophysics, Chandrasekhar (1961) on the stability of inviscid couette flow, and Phillips (1961) on centrifugal waves, plus many others. In all this time there have been only two experimenters who have interjected observational fact into the well-worked physical theory.

Fultz (1959) studied the axisymmetric inertial modes of a cylinder of fluid in solid body rotation, the first and most simple example given by Kelvin (1880). The agreement between theory and experiment was excellent. Phillips (1960) studied the stability and some normal oscillations of a hollow cylinder of fluid which had a high angular velocity about its central axis. The local gravity vector was perpendicular to the axis of rotation. He reported observations of two-dimensional azimuthal waves which agreed fairly well with the approximate theory. The paucity of experimental results arises from the technical difficulties encountered in attempting to observe complex three-dimensional waves within a rotating frame. In this experiment we have been forced to attempt quantitaive measurements of the oscillations of a complex annular vortex.

3.2 An Axisymmetric Annular Vortex (Kelvin's General Problem)

A rotating axi-symmetric source-sink flow such as ours consists of three types of motion: a two-dimensional, annular vortex bounded by Ekman layers on axial surfaces and two different shear layers on the outer (source) and inner (sink) porous walls (Figure 1A). Hide (1968) has recently described such systems from the stand-points of physical theory and observations, so the reader is referred to this work for the detailed argument applicable to the steady motions.

In this experiment we are concerned with the state of a source sink flow which has oscillatory Ekman layers The mean state of motion of the core vortex is two-dimensional and axisymmetric, but the existence of non-steady components considerably alters the picture gained by the steady state linear theory as we shall see in the next

sections. The major part of the volume of the annulus is occuppied by the inviscid vortex. In the course of this work experimental techniques became more refined, and it became apparent that the core was responding to the motions of the boundary layer in a coherent way. This realization motivated a study of the linear problem of the normal oscillations of a rotating annular vortex, which was the problem posed by Kelvin in 1880. Alas, after many days of mathematical divagations this author has learned, as many others have, that this eigenvalue problem cannot be solved by easy analytical methods. In the remainder of this section we shall state Kelvin's general problem of the annular vortex in a new way and shall try to surmise some implications from simple approximations. In section five we shall see that a complete solution is necessary to determine the role of the vortex in a general scheme of the source-sink motion.

3.3 Equations of Motion

In the following derivation of the pressure perturbation equation for linear vortex motion, we shall spare many details, since this is for most part a classical problem and a restatement of Kelvin's (1880) derivation in a rotating frame of reference. The importance of centrifugal constraints will become apparent where the discriminant for stability is recast in a rather novel way.

The momentum and continuity equations for a system in uniform rotation (Ω) about the z-axis are:

$$\frac{\partial \vec{u}}{\partial t} + (\vec{u}\cdot\nabla)\vec{u} + 2\Omega\vec{K}\times\vec{u} = -\frac{1}{\rho}\nabla p; \qquad \nabla\cdot\bar{u} = 0 \tag{3.1}$$

Where the reduced pressure (p) is given by:

$$p = \bar{P} + p' - \frac{1}{2}\Omega^2 r^2 \tag{3.2}$$

$\overline{P}$ is the mean ambient pressure, p' is fluctuating pressure perturbation, and $\frac{1}{2}\Omega^2 r^2$ is the centrigual force. In the core of axisymmetric source-sink flow, the mean ambient reduced pressure gradient is balanced by the coriolis force, and as a result there is a differential zonal vortex flow $\overline{V}(r)$ which is a function of the radial co-ordinate only. (See Hide, 1968.) In this problem we are interested only in the small time dependent fluctuations about the mean zonal state which are periodic in time, the azimuthal (zonal) and axial directions.

3.3.1 Perturbations and Scaling

The perturbations, which we shall assume to be much smaller than the mean, zonal motion, are to be scaled with respect to the radius (a), the height (H) of the annulus, and the rotation rate (Ω). The non-dimensional form of the independent variables in cylindrical coordinates can then be given as:

$$(3.3) \quad R = \frac{r}{a}\ ,\ \eta = \frac{z}{H}, \quad \theta = \theta, \quad \tau = \Omega t$$

The perturbations shall have the form, $\Omega a[F(R)\exp i(n\tau + m\theta + K\eta)]$, where n, m, and K are the non-dimensional frequency and wave numbers, respectively. Then the perturbations are:

$$(3.4) \qquad u = \Omega a[\psi(R)\exp i(n\tau + m\theta + K\eta)]$$

$$V = \Omega a[\chi(R)\exp i(n\tau + m\theta + K\eta)]$$

$$W = \Omega a[\Xi(R)\exp i(n\tau + m\theta + K\eta)]$$

$$P = \rho\Omega^2 a^2[\Sigma(R)\exp i(n\tau + m\theta + K\eta)]$$

$(\overline{V}(R) + V)$ - the total zonal component where at a given R, $(u, V, W,) << \overline{V}(R)$.

If we neglect squares and product of small quantities, substitutions of (3.3) and (3.4) into equations (3.1) will give us the following set of differential equations for the motion:

$$(3.5)\qquad i(n + m\varepsilon)\psi - 2(1 + \varepsilon)\chi = -D\Sigma$$

$$(RD\varepsilon + 2\varepsilon)\psi + i(n + m\varepsilon)\chi = -\frac{im\Sigma}{2R}$$

$$i(n + m\varepsilon)\Xi = -iK\Sigma$$

$$\frac{1}{R}\psi + D\psi + \frac{im}{R}\chi + iK\Xi = 0$$

where $D = d/dR$ and $\varepsilon = \bar{V}/\Omega a$, the Rossby number of the mean zonal flow at a given radius; later we shall refer to this quantity as the local Rossby number R_{OL} ($R_{OL} = \varepsilon$).

3.3.2. The Complete Equation for the Perturbation Pressure

Simultaneous solution of the first two equations of (3.5) gives χ and ψ in terms of $D\Sigma$ and Σ. These relations plus the axial velocity equation may be substituted into the continuity equation to obtain a differential equation for the oscillatory pressure perturbation:

$$(3.6)\qquad D^2\Sigma + \left[\frac{1}{R} - \frac{D(\Phi - \sigma^2)}{(\Phi - \sigma^2)}\right] D\Sigma +$$

$$\left\{\frac{2m}{\sigma R}\left[\frac{D\sigma}{m} - \frac{D(\Phi - \sigma^2)}{(\Phi - \sigma^2)}\right] - \frac{m^2}{R^2} + K^2\left(\frac{\Phi - \sigma^2}{\sigma^2}\right)\right\}\Sigma = 0$$

where $\sigma = n + m\varepsilon$, which we shall call the apparent frequency; the other new term Φ is the Rayliegh discriminant defined as:

$$(3.7)\qquad \Phi \equiv 2(1 + \varepsilon)[2(1 + \varepsilon) - R\, D\varepsilon]$$

3.3.3 The Rayliegh Discriminant

Lord Rayliegh (1920) showed that a necessary and sufficient condition for the stability of a steady rotating flow is that the radial gradient of the total circulation in the inertial frame must be positive ($\Phi > 0$), (see Chandrasekhar 1961, p. 275). In this experiment we have confined ourselves to the centrigually stable cases for which $\Phi > 0$. In equation 3.6 there are singularities when the Rayliegh discriminant equals the apparent frequency (σ). In his study of inviscid couette flow Chandrasekhar (1961) showed that centrifugally stable systems have

no real vertical wave numbers (K), if the apparent perturbation frequency σ is greater than or equal to the Rayliegh discriminant. Chandrasekhar arrived at his conclusion via a variational argument in which he had assumed that the radial component of the perturbation vanished (ψ=0) at the radial boundaries.

The condition that $\Phi > \sigma$ is not easily recognized until it is put into a form which is more familiar to the reader. We shall take the example of solid body rotation of an annular column of fluid where $\varepsilon = 0$, then

$$\Phi = 2(1+\varepsilon)[2(1+\varepsilon) - RD\varepsilon] = 4 \tag{3.8}$$

$$\sigma = n + m\varepsilon = n$$

So that Chandrasekhar's condition for real K (vertical eigenvalues) becomes the familiar relationship for limiting frequency of inertial waves of frequency n, $4 > n^2$.

Now let us attempt to gain some insight into the effects which differential rotation in a system may change the upper bound on the eigenfrequencies of the normal modes. In terms of the systems parameters the stability condition is:

$$-(\Phi^{1/2} + m\varepsilon) < n < (\Phi^{1/2} - m\varepsilon) \tag{3.9}$$

The first easily noted difference between the solid body frequency limit and the limit for this system with differential rotation is the dependence on the local Rossby number (ε) and the zonal wave number (m). As an illustrative example, let us assume that $\varepsilon = \frac{A}{R^2}$, then (3.9) takes the form:

$$-[2\sqrt{1 + 3\varepsilon + 2\varepsilon^2} + m\varepsilon] < n < [2\sqrt{1 + 3\varepsilon + 2\varepsilon^2} - m\varepsilon] \tag{3.10}$$

or in the case $\varepsilon << 1$, we can make the following approximation.

$$-[2 + (3 + m)\varepsilon] < n < 2 + (3 - m)\varepsilon$$

Thus we can see that at small Rossby numbers the characteristic frequencies corresponding to zonal wave numbers $m \leq 2$ are slightly higher than the solid body modes, while at higher mode numbers the maximum frequencies are lower. As Rossby number is increased to very large values, this stability condition restricts the zonal wave number to $m \leq 3$ for progressive ($n>0$) disturbances which move in the direction of the system rotation. The maximum allowable frequencies for the progressive waves is $n_{max} < (2\sqrt{2} - m)\varepsilon$, $m \leq 3$. If eigenmodes do exist for this vortex, then we should observe only the lower zonal wave numbers in the progressive waves. In observations of the core waves in the annulus we find that the dominant modes appear to have zonal wave numbers $m = 1$, $m = 2$ (section 4.3). The eigenfrequencies for a system can be calculated only if the boundary conditions are specified, so we shall discuss some of the plausible types which could be applied to solve equation 3.6.

3.3.4 Boundary Conditions

The first boundary condition which we shall assume is homogeneous at both radial boundaries. We shall require that the radial component of the perturbation (ψ) vanishes at the inner ($R = L$) and outer ($R = 1$) boundaries; in terms of the pressure these conditions are:

$$(3.10) \qquad \psi(b),\ \psi(1) = 0 = (n + m\varepsilon)D\Sigma + \frac{2m(1+\varepsilon)}{R}\Sigma$$

Chandrasekhar (1961) assumed these boundary conditions in the discussion on the stability of inviscid couette flows. Using these boundary conditions and a tacit assumption that the super-imposed motion was potential flow ($\varepsilon \propto \frac{1}{R^2}$), he arrived at a variational solution for the boundary

value problem specified by equations (3.6) and 3.10).

Another reasonable and relatively simple boundary condition allows small, periodic fluctuations of the radial components on a steady pressure surface; this is analogous to a compliant boundary or a free surface. In our annulus this condition could correspond to a fluctuating vertical shear layer, such as the sink boundary layer or the Ekman instability zone.

The net pressure fluctuations at the inner boundary (R=b) are

$$(3.11) \qquad \frac{p'}{\Omega^2 a^2} = [(R^2-b^2)+ (R)\exp i(n\tau + m\theta + K\eta)]$$

and the virtual fluctuations at the boundary are assumed to be given by;

$$(3.12) \qquad R = b + \Delta(R)\exp i(n\tau + m\theta + K\eta), \quad b>>\Delta(R)$$

so that the fluctuating pressure at the wall may be approximated to $0(\Delta)$ by;

$$(3.13) \qquad \frac{p'}{\Omega^2 a^2} = (\Sigma(R) + 2b\Delta(R)]\exp i(n\tau + m\theta + K\eta)$$

In the mean these small fluctuations must conform to the ambient pressure on the boundary at R = b, which we shall take to be zero, thus:

$$(3.14) \qquad \frac{p'}{\Omega^2 a^2} = \Sigma(R) + 2b\Delta(R) = 0 \quad \text{at } (R = b)$$

Kinematics of the small radial fluctuation requires that the fluid particles must follow the deformed radius, R. The motion following the fluid particles gives us the second part of the boundary condition approximated from

$$(3.15) \qquad \psi(R) \approx (\frac{\partial}{\partial\tau} + \frac{\varepsilon\partial}{b\partial\theta}) R = i(n + \frac{m\varepsilon}{b}) \Delta(R), \quad b>>\Delta(R).$$

The kinematic plus dynamic conditions at the boundaries to the $0(\Delta)$ approximation are

$$(3.16) \qquad \begin{cases} \psi(1) = 0 = (n + m\varepsilon(1)D\Sigma + 2m(1 + \varepsilon), & \text{at } R = 1 \\ \Sigma(b) + 2b\Delta(b) = 0 & \\ \psi(b) - 2[n + \frac{m\varepsilon(b)}{b}]\Delta(b) = 0 \} & \text{at } R = b \end{cases}$$

These non-homogeneous boundary conditions lead to very complicated eigenvalue relations, which cannot be resolved even for the most simple case of solid body rotation, by this writer. The following example will illustrate some of the difficulties which arise in the most simple case, solid body rotation of a fluid in a rigid annular container.

3.4 The Normal Inertial Modes of an Annular Column of Fluid

We shall assume that the radial and axial walls of our container are rigid, and that the fluid is in a mean state of solid rotation. The pressure equation (3.6) and simplified boundary conditions from (3.10) reduce to a Sturm-Liouville system with "separated" boundary conditions:

$$(3.17) \qquad D^2\Sigma + \frac{1}{R}D\Sigma + \left[\frac{K^2(4 - n_2)}{n^2} - \frac{m^2}{R^2}\right]\Sigma = 0$$

$$D\Sigma + \frac{2m}{R}\Sigma = 0 \quad \text{at } R = b \text{ and } 1$$

The eigenfunction must be a linear combination of Bessel's functions of the first and second kinds,

$$(3.18) \qquad \Sigma(R) = AJ_m(\kappa R) + BY_m(\kappa R)$$

$$(3.18b) \qquad \kappa = \frac{K^2(4-n^2)}{n^2}$$

in order that the conditions at the inner and outer boundaries are satisfied. The coefficients, A and B, are determined to an arbitrary amplitude by substitution of this eigenfunction into the boundary condition at R = 1, then (3.10) $\Sigma(R) = A[J_m(\kappa R) - \frac{(2+n)Y_{m-1}(\kappa) + (2-n)Y_{m+1}(\kappa)}{(2+n)J_{m-1}(\kappa) + (2-n)J_{m+1}(\kappa)} Y_m(\kappa R)]$ The reader will find that the following relations are necessary to obtain equation 3.19:

$$(3.20) \qquad \frac{2m}{\kappa R} J_m(\kappa R) = J_{m-1}(\kappa R) + J_{m+1}(\kappa R)$$

$$\frac{2}{\kappa} DJ_m(\kappa R) = J_{m-1}(\kappa R) - J_{m+1}(\kappa R)$$

The relationships among n, m, k, and κ is obtained by substitution of (3.19) into the boundary condition at the inner wall (R = B); after more manipulation we find the transcendental equation,

$$(3.21) \qquad \frac{J_{m-1}(\kappa b) + \beta J_{m+1}(\kappa b)}{J_{m-1}(\kappa) + J_{m+1}(\kappa)} = \frac{Y_{m-1}(\kappa b) + \beta Y_{m+1}(\kappa b)}{Y_{m-1}(\kappa) + Y_{m+1}(\kappa)}$$

where $\beta = (\frac{2-n}{2+n})$. A Sturm-Liouville system of this stype has a denumerable infinity of eigenvalues. The unwieldy relationship for this most simple example of three-dimensional waves stymies a smooth quantitative solution for the eigenvalues of a given container.

3.41 An Approximation of Eigenvalues

In equation 3.18 we defined the eigenvalue, (κ) which is a function of the vertical wave number, $K = q2\pi a/H$, (q = 1, 2, 3 ...) and the nondimensional frequency (n). From this definition we can see that the smallest eigenvalues ($\kappa \geq 0$) corresponds to n~2, and that $\kappa \to \infty$, as $n \to 0$. Physically the eigenvalue corresponds to a measure of the number of nodes in a radial standing wave decribed by its eigenfunction, so that large κ means that there are many undulations between the radial boundaries. The aspect ratio, a/H, and the distance between walls, a(1-b), are important in the determination of κ. When the aspect ratio and the distance between walls is large, κ may be large for relatively high frequencies; in these cases we can call on some well known approximations for eigenvalues of Scapital systems with separated boundary conditions.

If κ_α is the αth eigenvalue for our system equations and α is a large number, then κ_α can be estimated (see Birkhoff and Rotta, 1962) to $0(\frac{1}{\alpha})$ by

$$\kappa_\alpha \approx \frac{\alpha\pi}{1-b} - \frac{1}{\alpha} \tag{3.22}$$

$$\kappa = \frac{K(4-n)^{1/2}}{n} \tag{3.18}$$

In this experiment (section 4.2.1) we have determined that the most energetic waves in the core vortex have non-dimensional frequencies, $n \sim 0.38$ and 0.86. The eigenvalues κ associated with these frequencies by equation 3.18 are $\kappa_1 = 80.5$ and $\kappa_2 = 28$, respectively. We can then see whether the approximation (3.22) holds in these cases:

$$\alpha_{\kappa 1} \approx 23$$

$$\alpha_{\kappa 2} \approx 8$$

α is not large. This indicates that these frequencies could possibly correspond to some of the higher frequency modes of the annulus, however the observed oscillations do not appear to have the high numbers of nodes indicated from equation 3.18.

3.5 Commentary on Future Work

The complete pressure equation 3.6 may be integrated by numerical methods with reasonable ease, but the complexities of the boundary conditions may create some difficult problems. The normal frequencies of annuluar cylinder can also be calculated using a high speed computer which is programmed to search for the zeros of equation 3.21. Both of these projects are necessary and worthwhile to the clear interpretation of the body of data obtained in this experiment; however, they must be deferred to a time in the near future. Problems, which have awaited solutions for nearly a century, can wait a while longer.

4.0 Results

4.1 Correspondence of Boundary Layer and Core Motion

Initial observations in the experiment lead to the conclusion that the energy sources for the oscillations observed in the interior were the instabilities associated with Ekman layer transitions. In order to check this conclusion it is necessary to establish the sequence in which the boundary layer instability and the core motions appeared. This sequence is determined in the following manner:

1. At a constant rotation rate the flux is set so that no oscillations distinguishable from a low ambient noise level are detected by either of two sensors; one of which is in the Ekman layer at the edge of the sink boundary layer, and the other is at mid-radius in the core.
2. Flux rate is increased until fluctuations are observed at the inner sensor, since the boundary layer appears to be most unstable within the region near the sink.

The sequence established in this manner shows that the boundary layer instabilities preceed the interior oscillations. The core oscillations appear to grow to full amplitude within less than two rotation periods after the onset of boundary layer oscillations.

If the flux is increased past this incipient interaction level, the first Ekman instabilities occur at larger radii which broaden the areas of the perturbation sources, and their frequency bands.

Once motion within the core is established, the fluctuating components in the Ekman layers have the same frequency spectra as the core. This indicates that the zonal oscillations are of a sufficient amplitude to affect the transitional properties of the Ekman Layer to the extent that the only unstable waves being generated are those which correspond to characteristic zonal modes.

4.2 Characteristics of the Zonal Waves

The zonal waves are periodic, persistent, and repeatable for a given radius at a set state of flux and rotation. The root mean square of these oscillationsvaries from less than 1% to about 7% when normalized against the mean zonal component; the ambient noise level is quite low at less than 1/2% in most cases.

The first observations of these waves taken as radial profiles showed that they were quite periodic, in fact the simple time averages of the observed periods of the fluctuations on the oscilloscope agreed well with the more sophisticated analog techniques employed later. In taking the profiles of the zonal velocity in the core one can see that the apparent frequency of the oscillations changes quite radically at various radii; spectral analyses of these motions show that they are superpositions of different modes which exist at most radii, but have differing amplitudes according to their radial mode numbers.

4.2.1 Amplitude Spectra

Examples of the distributions of frequencies of the time dependent motion are given in Figures 6 and 7(A). Figure 6 also shows the radial variations of the spectra and the frequencies in which two

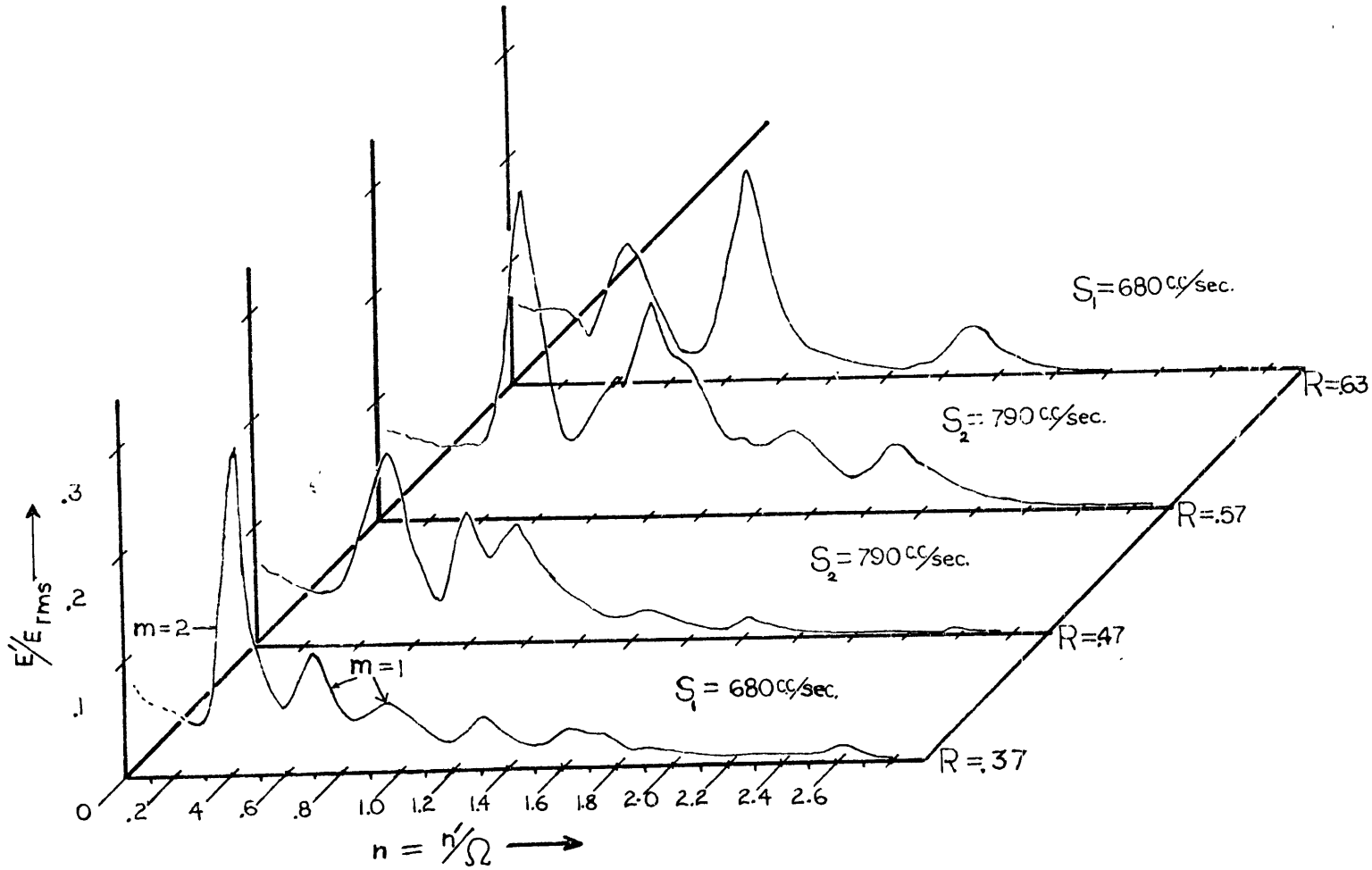

FIGURE 6

Amplitudes of normalized sensor voltage fluctuations ($E'/E_{r.m.s.}$) versus nondimensional frequency [n = n'/(3.55/sec.)]. Waves tend to slightly higher frequencies at higher flux (note R = .47 and R = .57).

azimuthal wave numbers m=1 and m=2 have been identified. The change of the amplitudes with radius indicate a radial variation for the major components which may be taken to indicate the presence of normal modes. In all spectra there is little motion detected at frequencies above 2Ω, the inertial limit for motions without differential rotation. Most of the energy in the oscillations is in a frequency band concentrated between 0.2Ω and $.95\Omega$ in both examples; however, there is evidence of lower frequency modes which lie beyond the resolution of the spectral analyzer employed in this stage in the experiment. Figure 7(A) shows the relations of the fluctuation spectra obtained by two sensors; the inner of which is within a transitional Ekman layer. The outer is well above the boundary. The inset, Figure 7B, is a sample of recorded voltage fluctuations taken at the inner and outer positions. The two traces have been synchronized using information from cross correlations of the signals. The significance of the lag or phase shift between inner and outer portions of the wave will be discussed in section (5). Figure 8 represents a summary of spectra taken at four radial locations at a moderately high Rossby number. The high frequency peaks ($>\Omega$) appear to be sums of lower frequency components ($\Omega<$) except for the sharp peak at 1.4Ω.

4.2.2 Relation of Rotation Rate and Flux to Observed Frequencies.

The frequencies of the dominant modes are found to vary with Ω as a linear function which has a slope of unity over the range $\Omega=2.09$ to 8.08 rad/sec.

Increase in the flux from source to sink generally leads to higher energies in the basic modes and has a tendency to increase the frequency

Spectra of fluctuations at two sensors, where the inner sensor (R = .35) is within a transitional Ekman layer, and the outer is within the core.

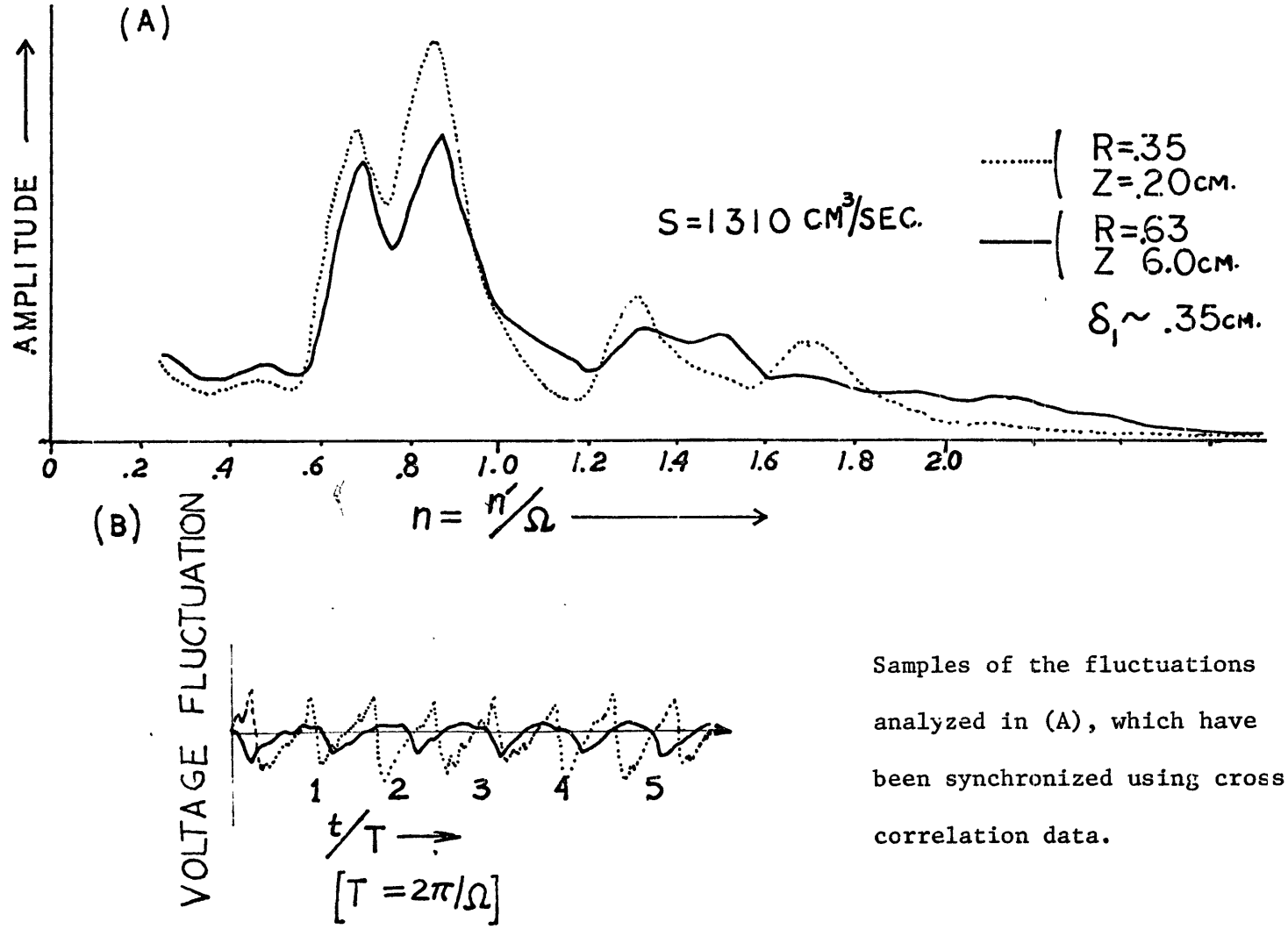

Samples of the fluctuations analyzed in (A), which have been synchronized using cross correlation data.

FIGURE 7

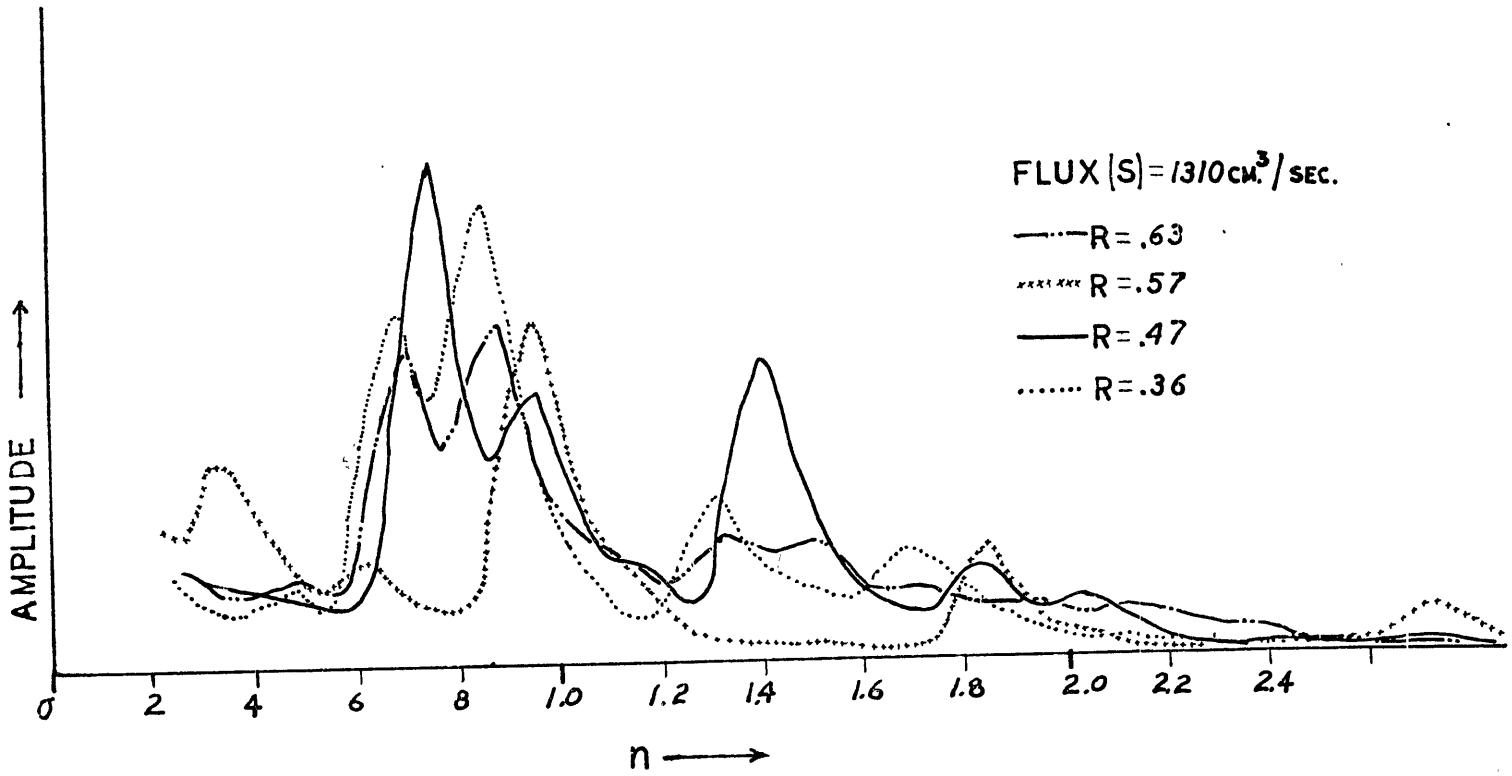

FIGURE 8 Fluctuation amplitudes at various radii versus non-dimensional frequency(n).

of a given mode. See Figure 6, R = .47 and .57. This frequency shift is attributable to the increase in zonal advection of the wave field by the mean motion.

4.2.3 Correlations of the Fluctuations.

Voltage fluctuations from the velocity sensors were correlated in the correlation function computer (Section 2, Figure 2). Auto correlation functions obtained show that most components of the oscillatory motion are highly coherent in time, and in most cases the waves appear to be superpositons of sine waves moving at different, but constant, phase velocities (See Figure 9A and B). In most cases, such as the cited figures, the periods between maxima in the auto correlations correspond to the peaks in the observed spectra. The envelope in Figure 9A corresponds to the difference beat and summing beat of the two dominant modes.

Cross correlations of the fluctuations show that the waves move as coherent entities as they progress from one spatial point to another. The distinctiveness of the dominant modes allows the measurement of the time required for a given component wave to move from one point to another. The azimuthal velocities of identifiable components are measured by obtaining the time delay to maximum cross correlation of the fluctuations from two sensors set at the same axial position and radius but separated by a knownazimuthal distance; the velocity is then the distance divided by the time delay (Figure 10). The frequency of the component may be determined from the spectra and the auto correlations. The angular frequency divided into the apparent frequency should give the

The predominant waves appear to interfere with each other causing this continuous modulation of the correlation functions.

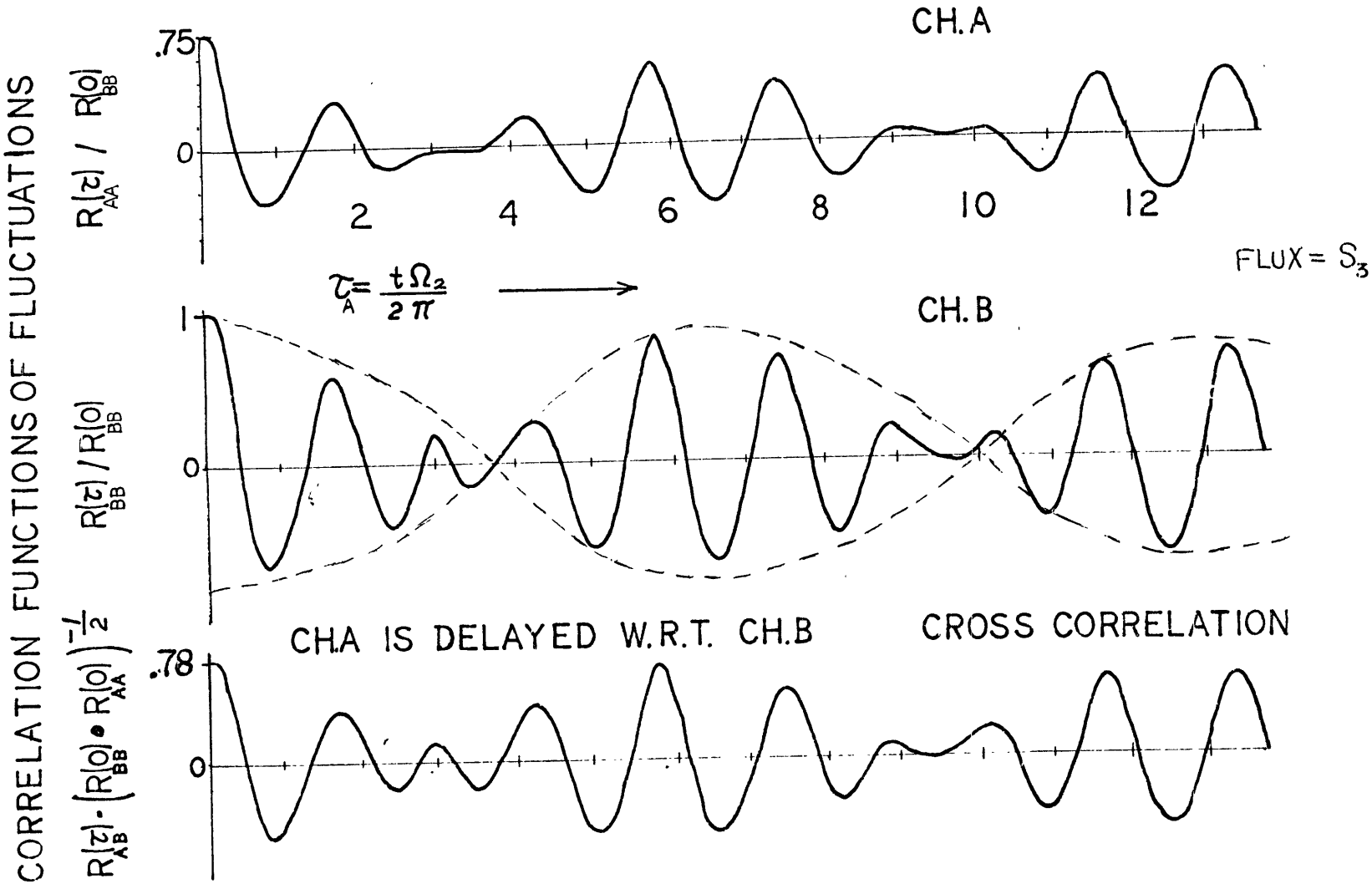

FIGURE 9 Correlations of fluctuations. Sensors radially aligned separation .27R.

azimuthal wave number of the mode. Examples of wave number determined in this manner are noted in Figure 6. In less distinctive cases, or where accurate determination of the relative phase lag is to be determined, the component of interest is filtered. In Figure 11 fluctuations at two different radial positions have been filtered at the frequency associated with a component of azimuthal wave number m = 1 at two different flux rates. The sensors are aligned radially; however the inner sensor in each case is submerged in a transitional Ekman layer and the outer is within the core flow. There is a steady lag of nearly 180° between the two signals; from this we can surmise that the wave motion in the Ekman layer is syncopated with the motions of a radial standing wave in the core.

Cross correlations of components at different axial positions show that there is definite vertical structure in the waves; however, the coarseness of the spatial separation between the sensors only allows a qualitative appraisal of the vertical wave number at a given frequency. This rough estimation shows that the mid-axial plane between the horizontal disks is the nodal point for the dominant progressive modes of azimuthal wave numbers m = 1 and m = 2.

In addition to the progressive waves there are retrogressive waves; the only component of this type which can be identified with certainty at this time has an azimuthal wave number m = 1 and frequency of 0.65Ω in figure 6. The amplitude of this mode decreases rapidly at the outer radii.

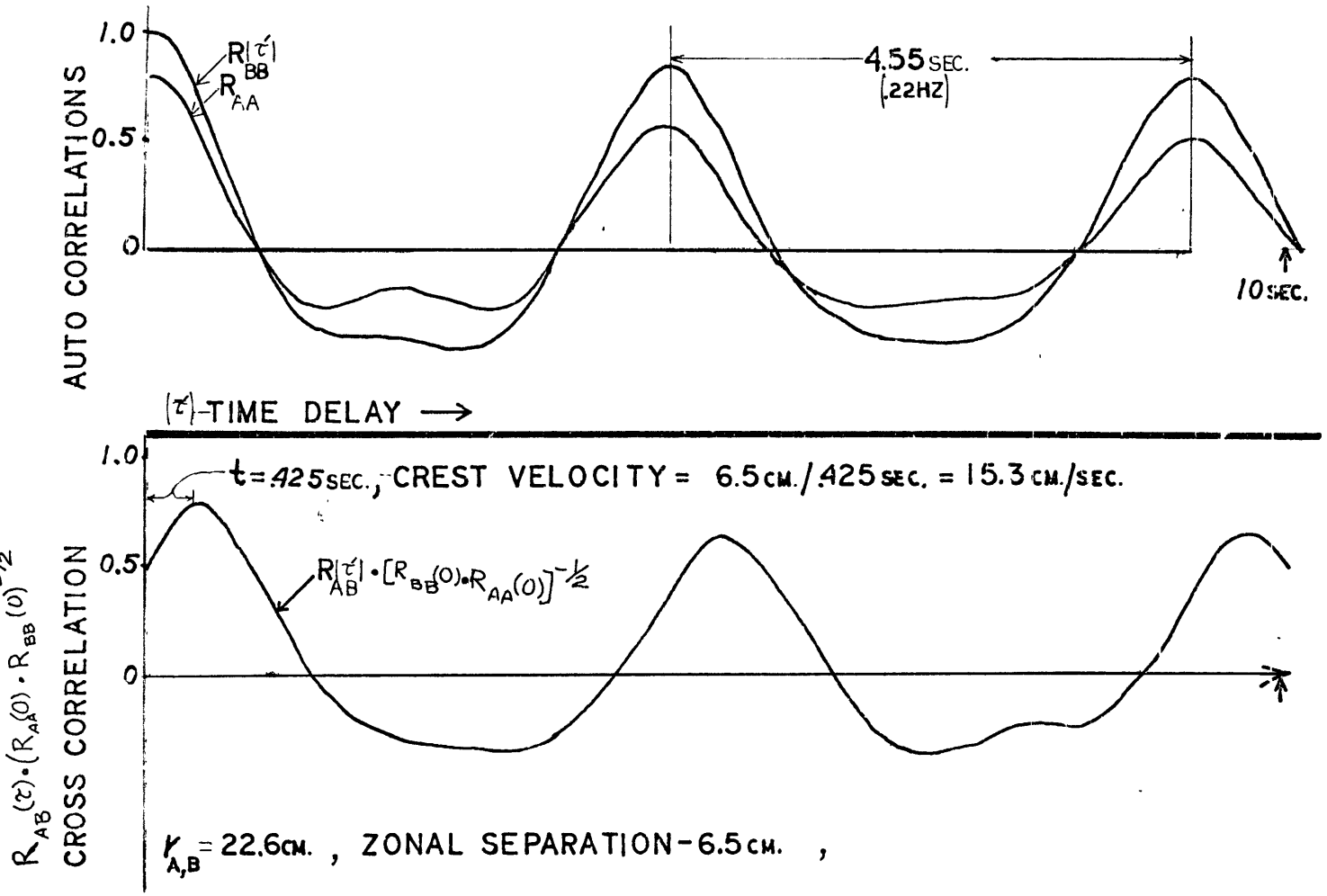

Determination of zonal wave number

FIGURE 10

A wave with a crest velocity of 15.3 cm./sec. at a radius 22.6 cm. from the axis would have a frequency of 0.11 Hz, if there were only one crest. However the observed frequency is .22 Hz, so there must be 2 crests ($m = 2$). The waves with m = 1 were also identified in this manner.

In cases A and B the sensors are separated by a distance of .27R. The inner sensor is within a transitional Ekman layer, and the outer, which is delayed with respect to the inner, is within the core (R = .63, z = 6cm.). The center frequency of the filters are set at n = .86 which corresponds to the progressive wave m = 1.

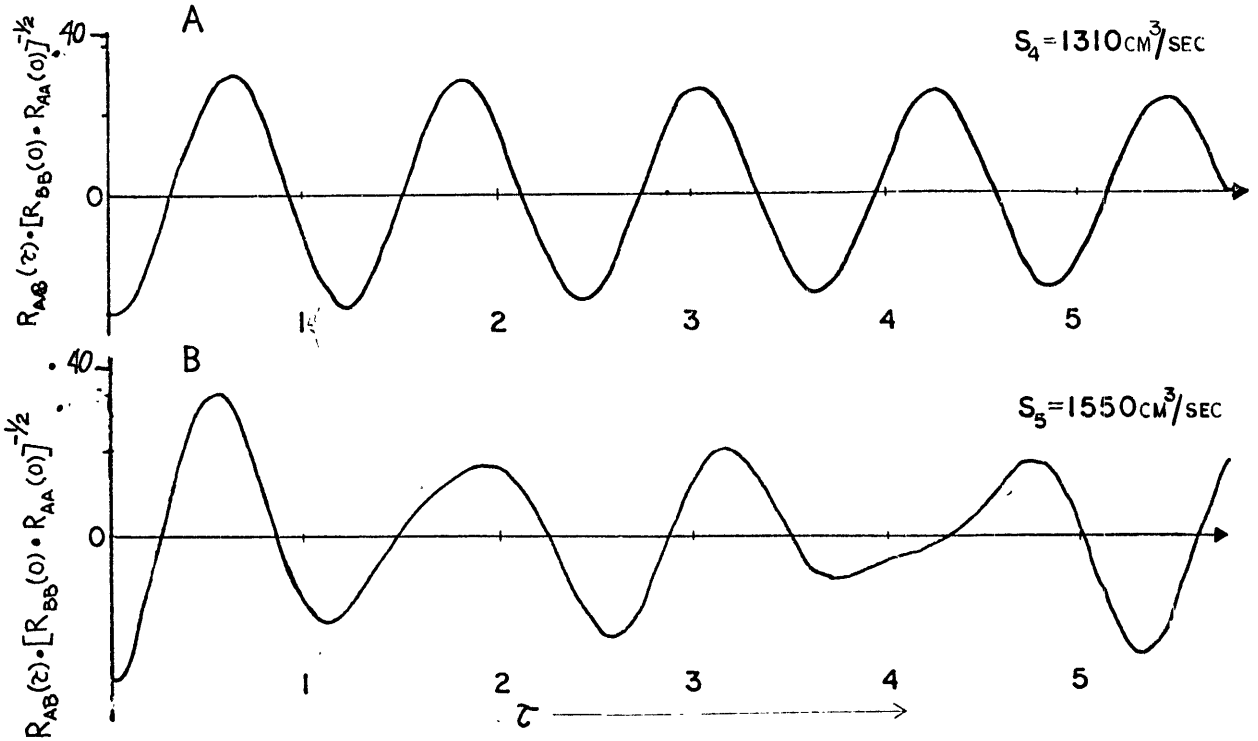

FIGURE 11 Filtered cross correlations between fluctuations.
(The time delay(τ) is non-dimensionalized by the rotation period)

4.3 The Mean Motion

4.3.1 The Mean Zonal Profiles

The mean zonal motion in the core of the annulus is two dimensional and axi-symmetric. There is no detectible axially-dependent variation of the mean except in the Ekman Layers and the source and sink layers. A number of radial profiles of the mean zonal velocities were obtained for various states of volume flux (s) and rotation rates (Ω). These data were used to compute the nondimensional relative circulations of the zonal means, which are presented in figures 13 and 14. In both of these figures there are profiles in which the radial dependence of the circulations are rather marked over a sizable portion of the radius, and in most cases this dependence is linear. The slopes of these gradient circulations are dependent on the system Rossby number R_{OS}, which must be constant over the sloping radial interval. This parameter is related to the local Rossby number, and nondimensional circulation by

$$(4.1)\quad \Gamma = \frac{\overline{V}R}{\Omega a} = R^2 R_{OL} = R R_{OS}$$

$\overline{V}$ = the measured zonal mean velocity at R.

R = Non-Dimensional radius (r/a)

R_{OL} = the local Rossby number ($\overline{V}/\Omega aR$)

R_{OS} = the system Rossby number ($\overline{V}/\Omega a$)

The slope of the circulation profile determines the vertical component of the mean vorticity (ξ) since

$$(4.2)\quad \frac{1}{R} D\Gamma = \overline{\xi}$$

The profiles which have a positive slope are indicative of mean states of positive (cyclonic) relative vorticity. These positive vorticity portions of the core exist at the outer radii and surround a portion of the core which has constant circulation. At moderate to high levels of

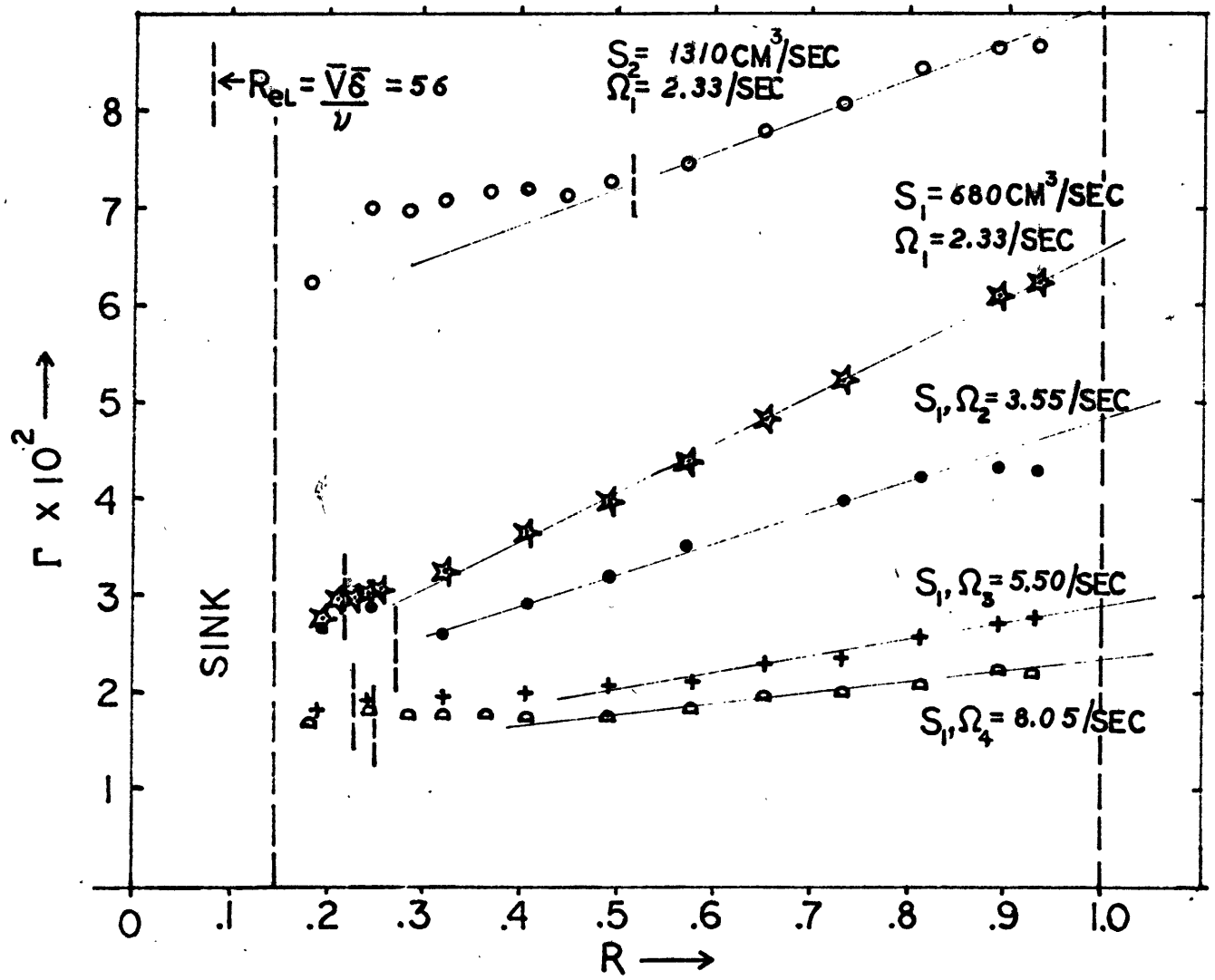

(FIGURE) 12 Non-dimensional circulation (Γ) versus non-dimensional radius (R).

flux (S) or rotation rate (Ω) the positive vorticity portions of the zonal mean decrease in width and proceed toward the outer wall. The significance of these states will be discussed in section 5.

No examples of centrifugally unstable profiles were seen in the recorded data (3.2), however in the high Rossby number ranges, the sharply sloping circulation near the source indicates that a state of unstable shear flow may exist there.

4.3.2 Comparisons with Other Experiments.

The two experiments known to this author which can be compared to the present work were conducted by Faller (1963) and Tatro and Mollo-Christensen (1967). Although the apparatus in the latter experiment is identical in basic design to that employed here, no data are published which provide sufficient information about the control parameters used in the one mean profile of zonal velocity they presented. This profile is similar to those obtained at moderate rotation rates and flux in our experiment. The thicknesses of the Ekman layers in the Tatro and Mollo-Christensen experiment were somewhat greater than the standard scale of $(\nu/\Omega)^{1/2}$ for Ekman thickness. This phenomenon is also observed in this apparatus.

Faller (1963) studied the properties of some of the more stationary modes of the higher Reynold's number instability in a shallow rotating tank with a free surface. The water source was distributed around the lower rim at the outer radius, and the sink was at the center. This experiment cannot be compared directly to this experiment since the critical similarity variables R_{OL}, R_{eL} and $E^{1/2}$ cannot be made equal simultaneously

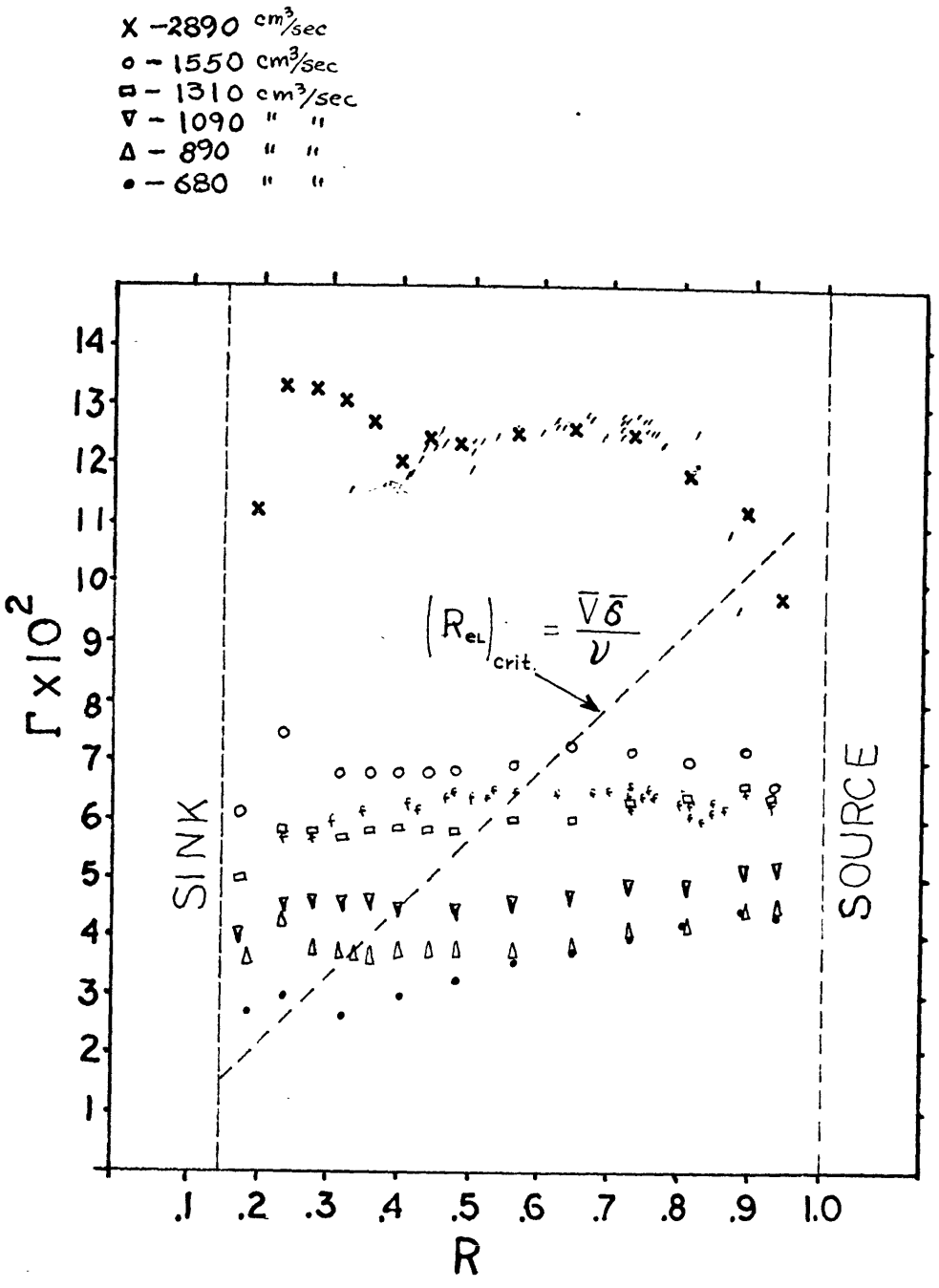

FIGURE 13 Non-dimensional circulation (Γ) versus non-dimensional radius (R). Here flux (S) is varied while Ω is held constant ($3.55 \pm .04$/sec). The points marked by (f) and (/) are transcribed from Faller (1963) exp. 29. iii. 60, III and IV. Faller's data represent circulations at higher Reynolds and Ekman numbers. (4.3.2)

due to the differences in the kinematic viscosities of air and water plus the variation of aspect ratio in the tank with a free surface. A Rossby number based on the system variables was chosen as the most suitable modeling parameter in the comparison where,

$$(4.3) \qquad R_{OL} = \left[\frac{S_f}{\pi a^2 {}_f\Omega^{1/2} \nu_{H_2O}^{1/2}} \right] \frac{1}{R^2} = \frac{S}{2\pi a^2 \Omega^{1/2} \nu^{1/2} R^2} \quad .$$

The "f" subscripts denote Faller's scale values. In figure 14 some of Faller's data points are superposed on the non-dimensional circulation profiles. The agreement is good at the higher Rossby numbers, but the asimiliarity of Reynolds number and Ekman numbers is reflected in the difference in slope at the lower circulation.

4.3.3. Measurements of the Mean Ekman Thickness

Measurements of the thickness of the Ekman layer are made at seven radial positions across the lower boundary of the annulus at the same rotation and flux rates (Ω = 3.44 rad/sec and S = 680 cc/sec). There is not detectible variation of the boundary layer thickness, except in the confluence of the Ekman layer and the vertical sink layer. Two definitions of thickness were used; both agreed within 6% of their mean. The first type is a measure of the axial distance (z) above the boundary at which detectible variation of the zonal component with axial displacement is zero to our best determination.

The second is computed from the observed displacement of the mean maximum of the radial component of the boundary layer from the boundary:

$$(4.4) \qquad \delta_2 = \frac{4Z}{\pi}$$

Using these definitions at the six outer radii we obtain:

$$\delta_1 = .36 \pm .02 \text{ cm}$$

$$\delta_2 = .34 \pm .02 \text{ cm}$$

The major uncertainties in these measurements arise from indeterminate lower boundary positions (z=0), since the hot wire sensors respond to the proximity of the heat conducting boundary unpredictably at the low velocities encountered.

The standard scale Ekman thickness for a steady laminar boundary layer is

$$d = \sqrt{\frac{\nu}{\Omega}} = 0.208 \text{ cm}$$

In this case Ω =3.55 rad/sec and ν= .155 $\frac{\text{cm}}{\text{sec}}$. The mean measured boundary layers are then thicker by the ratios,

$$\frac{\delta_1}{d} = 1.73 \pm .09$$

$$\frac{\delta_2}{d} = 1.63 \pm .09$$

The Ekman layer is not distinct within the sink layer, it is coupled to the sink by a strongly oscillatory transition flow. The strongest fluctuations in this region occur at z/d $\approx$ 3.

Two other thickness measurements have been made at central radii. The rotation rate is the same as before, but the flux has been increased to 1550 cc/sec. No changes in thickness are detected.

4.4 Ekman Layer Transition.

Tatro and Mollo-Christensen (1967) determined the transition parameter for the lower Reynolds number Ekman instability (see section 5) in terms of the local Reynolds number ($R_{eL} = \frac{\overline{V}\delta_2}{\nu}$) and local Rossby number (R_{OL}). Most of these measurements were made near mid-radius at

fixed states of rotation and variable flux rates. Their results of observations of a number of transitions yielded the following empirical relation between critical Reynolds number and Rossby number:

$$(4.5) \qquad (R_{eL})_{crit} = 56.3 + 58.4\ (R_{OL})_{crit}$$

Transitions of the Ekman layer are observed in this experiment which do not have this linear dependence of critical Reynolds number on the Rossby number; however boundary layer transitions are observed at a Reynolds number,

$$(R_{eL})_{crit} = \frac{\overline{V}\delta_2}{\nu} \sim 56$$

The difference is not really contradictory, when the basic definitions of R_{eL} and R_{OL} are considered;

$$R_{eL} = \frac{\overline{V}\delta_2}{\nu} \quad , \quad R_{OL} = \frac{\overline{V}}{\Omega a R}$$

so that:

$$(4.6) \qquad R_{OL} = \frac{\nu}{\delta_2 \Omega a R} R_{eL}$$

The empirical equation (4.5) by Tatro and Mollo-Christensen becomes:

$$(R_{eL} = 56.3 + \frac{58.4\nu}{\delta_2 \Omega a R_{crit}} (R_{eL})_{crit}$$

or,

$$(4.7) \qquad (R_{eL})_{crit} = \frac{56.3}{1 - \frac{58.4\nu}{\delta \Omega a R_{crit}}} = \frac{56.3 R_{crit}}{R_{crit} - 58.4 E^{1/2} \frac{d}{\delta_2}(\frac{H}{a})}$$

In this experiment the factor,

$$(58.4E^{1/2}\frac{d}{\delta_2}(\frac{H}{a}) < 2 \times 10^{-3} << R_{crit})$$

so that the radial variation of the critical parameter is unimportant.

5.0 Discussion

5.1 Resumé of Important Results

In the experiment we have learned several interesting properties of both the mean and oscillatory states of the non-steady source sink flow, and in this section we shall attempt to synthesize the results with the aid of physical reasoning. First we shall list the major results of observations and measurements:

1. Incipient Ekman layer instabilities are the primary energy sources for oscillations in the inviscid core of the vortex.
2. The core oscillations are three dimensional periodic waves.
3. The frequency spectra of the core and the transitional boundary layers coincide, suggesting that there is a feedback of information from the core to the boundary layer.
4. The mean Ekman layer thickness is considerably greater than the accepted value, $(\nu/\Omega)^{1/2}$, accountable to steady theory.
5. Some states of mean motion possess a net positive relative vorticity.

Now we shall start the synthesis of this information by determining a relationship between the first and last of the results in this list.

5.2 Ekman Layer Transition and Positive Vorticity States.

In [4.4] we found that the critical value for the boundary layer in this system is $R_{eL_{crit}} \sim 56$, and in [4.3.3] we observed that the Ekman layers have a mean thickness approximately $1.7(\nu/\Omega)^{1/2}$. Now we shall define a critical velocity $\overline{V}_c$ in the mean zonal flow for which the Ekman layer may have incipient instabilities, in terms of the

critical Reynolds number $(R_{eL})_{crit}$ and the local average Ekman thickness $\overline{\delta} = 1.7(\nu/\Omega)^{1/2}$:

(5.1) $$\overline{V}_c = \frac{\nu(R_{eL})_{crit}}{1.7(\nu/\Omega)} = 33\Omega^{12}\nu^{12} \text{ or } (R_{eL})_{crit} = \frac{\overline{V}_c\overline{\delta}}{\nu} = 56$$

$\overline{V}_c$ can be directly compared with the mean zonal velocity ($\overline{V}$) profiles. The radii at which $\overline{V}_c = \overline{V}$ are noted in Figures 13 and 14. The contiguity of the critical radii for Ekman instability ($R_{eL} = 56$) and the radii at which the gradients of the mean relative circulation die away indicates the phenomena are coupled. The greatest deviations of the measured transition radii from those predicted by this method occur at the higher rotation rates, indicating that the boundary layers may be thicker than the assumed value of $1.7(\nu/\Omega)^{1/2} = \overline{\delta}$.

Now we should recall that the gradient of the circulation is related to the mean vertical component of vorticity by

(4.2) $$\frac{1}{R} D\Gamma = \overline{\xi}$$

The derivative of the circulation is constant until the transition ($R_{eL} \approx 56$) occurs and in that region it ostensibly goes to zero; therefore the transition region is also the zone of maximum mean vorticity in the core. In terms of the mean motion, the presence of the cyclonic vorticity in the core must be balanced by a viscous diffusion and stretching of the axial vorticity component $\overline{\xi}$. This diffusion of vorticity from the core is balanced by advection of mass from the Ekman layers; at a given radius in the cyclonic region the mean axial velocity ($\overline{W}$) out of the Ekman layer is given by:

$$\overline{W} = E^{1/2}\,\overline{\xi}$$

In this experiment $E^{1/2}$ is $O(10^{-2})$ or less, and the maximum value of $\overline{\xi}$ is $O(10^{-1})$ so that the maximum axial velocities by this order approxi-

mation are very small (less than 0.06 cm/sec in the extreme case). From the available evidence we have been able to relate the local phenomenon of boundary layer instability to the existence of positive vorticity states in the mean core motion which have a considerably larger spatial scale. Oscillations in the inviscid core, which are caused by the unstable boundary layer appear to be the mechanism by which these two scales of motion are coupled.

5.3 Dissipation of Inertial Waves by Stable Ekman Layers

Incipient Ekman layer instabilities ($R_{eL} \sim 56$) produce a state of periodic, three dimensional motion in the inviscid core, and as a consequence all parts of the flow are forced to respond. The stable Ekman layers respond to the core waves with damped oscillatory motions. The interaction between inviscid modes and laminar Ekman boundary layers in contained fluids has been studied extensively from the standpoint of linear perturbation analysis by Greenspan (1968); however no models directly analogous to our system are available. A theoretical model for the interactions of inviscid normal modes of a cylinder with the viscous boundary layers has been presented by Kudlick [1966] who obtained expressions for the viscous corrections of the inviscid eigenvalues. Kudlick's results can be compared qualitatively with those obtained in this experiment when we consider the observed flows where the local Rossby number is small, local Reynolds number is below critical value ($R_{eL} < 56$) and the Ekman number is $O(10^{-5})$. Here the linear theory, which should be a good approximation, indicates that the modal waves are dissipated within the Ekman layers by viscosity. The net

effect of this dissipative process is an efflux of mass from the boundaries, which in the mean alters the state of interior vorticity. This forced motion of the Ekman layers effectively changes their depth scales by the axial flux. Unfortunately, Kudlick's eigenfrequencies do not correspond with our data from the annulus, and no explicit form for the eigenfunctions of the core oscillations yet exists, so the general theory cannot be applied.

5.4 The Coupling Mechanisms

5.4.1 Incipient Ekman Instabilities in a Non-Steady Circular Flow

Lilly [1966] determined that steady, nondivergent Ekman layers exhibit an instability at Reynolds number $R_e = \frac{\overline{V}}{\Omega^{1/2}\nu^{1/2}} \approx 55$. The instability waves were assumed to take the form of two dimensional vortex rolls which propagate along the Ekman layer at a small angle with respect to the direction of the mean zonal flow. In a cylindrical configuration such as ours these waves should propagate toward the center of the annulus. Lilly named this low Reynolds number instability the "parallel instability", since it appears to draw its energy from the mean zonal flow component through the axial gradient of the mean zonal component in the boundary layer ($\frac{d\overline{V}}{dz}$) and the fluctuating Reynolds stresses ($V'W'$). Lilly reasoned that these instabilities could grow only if the time average correlation (denoted by the bar) of these quantities is less than zero:

$$\overline{V'W' \frac{d\overline{V}}{dz}} < 0 .$$

An important feature of this instability is its decreasing growth rate with increasing Reynolds for a given disturbance, since the relative

strength of the Coriolis force decreases as advective forces become more important in the motion. The horizontal scale lengths of these disturbances range approximately from 22 to 35 boundary layer thicknesses $(\nu/\Omega)^{1/2}$ and an axial scale nearly $8(\nu/\Omega)^{1/2}$. The velocities of these waves range from $.3\overline{V}$ to $.62\overline{V}$ along the direction of the zonal flow.

Tatro and Mollo-Christensen (1967) made numerous measurements of these low Reynolds numbers instabilities within an annulus similar in basic design to ours. They found that the instabilities which they observed corresponded to those predicted by Lilly, if all scales of velocity and length were related to the local zonal velocity and the local boundary layer thickness δ_2 (see equation 4.4). They observed that the disturbances propagated toward the sink at angles from zero to 14° measured counter-clockwise with respect to the mean zonal velocity. They found, as we did, that the critical parameter is the local Reynolds number ($R_{eL} \gtrsim 56$). The major difference from the theory of Lilly and the observed disturbances appeared to be angular orientation of the most unstable waves to the zonal flow. Lilly predicted a clockwise angle of 20° at $R_e = 65$, but Tatro and Mollo-Christensen observed no wave with detectible clockwise orientation to the flow. In the same apparatus Mollo-Christensen, Tatro and Green (1966) later found that the onset of unstable motions in the boundary layer was associated with fluctuating motions in the interior. This is a crucial point.

Tatro and Mollo-Christensen had observed the instabilities of non-steady Ekman layers, not the steady, non-divergent types predicted by Lilly's theory. The effect of curvature played an important role and must have been an important constraint on the incipient instabilities.

The wave lengths of the disturbances observed by Tatro and Mollo-Christensen ranged from $22\delta_2$ to $33\delta_2$ while δ_2 varied from about 0.3 cm to nearly 1 cm, estimating from their published profiles. Assuming that these values are correct, the dimensional wave lengths of the disturbances they observed could range from 6.6 cm to about 30 cm. Their annulus had a radius of only 45 cm, so the observed wave lengths were of the same order as the radius of their apparatus.

In this experiment the waves observed in the inviscid core and the Ekman layers have a very definite azimuthal periodicity. This indicates that curvature of the interior flow is important to the characteristic response of the entire system to the forcing produced by the disturbed boundary layers. There is another point which has escaped comment by other authors namely the effect of increasing Reynolds number ($55 < R_{eL} < 110$) in a flow where this parameter is a function of one of the coordinates (R).

Once more let us recall that the mean zonal motion in the annulus is axisymmetric, and that the zonal velocity is roughly proportional to R^{-1}:

$$\overline{V} \propto \frac{1}{R}$$

Therefore the local Reynolds number R_{eL} is also $\tilde{\propto} R^{-1}$. This proportionality is most accurate at radii inside of the transition zone.

In our annulus the contours of constant Reynolds number are axisymmetric circles in the Ekman layers on the top and bottom boundaries. At some critical radius determined by the mean zonal velocity and the boundary layer thickness, the balance among the coriolis, pressure gradient, viscous, and local accelerative forces in the laminar non-steady

Ekman layers breaks down. Both Ekman layers are unstable at all points along the boundaries in board of the marginally critical transition zone ($R_{eL} \sim 56$). Each point along the radius ($R<R_{crit}$) is at a different Reynold's number. In light of Lilly's theory we should expect to see a slightly different dominant frequency and wave length at each radius since the local Reynold's number is a function of the radius with flux and rotation rate constant. Lilly found that the maximally unstable disturbances varied in growth rate approximately as the logarithm of R_{eL}, and that these waves could vary considerably in wave length and velocity over the range where they dominate nonlinear motions in the boundary layers ($R_{eL} < 125$). Instead of continuous distribution of unstable motions, we observe a rather coherent state with most of its energy concentrated in very narrow frequency bands. The boundary layer waves have the same frequencies as the oscillations within the interior. There are two good reasons for the highly organized appearance of the actual motions.

The first reason arises from the fact that the inviscid zonal motion is capable of storing information in terms of small fluctuations about its mean ($\overline{V} + V'$). It is possible that the core vortex has normal modes which resonate with the boundary layer disturbances. This hypothesis cannot be verified until equation 3.6 is solved with the appropriate boundary conditions. The incipient instabilities are particularly suited for coupling with the interior since they draw their energy from the mean zonal flow which is a balance of the coriolis and pressure gradient forces. Another factor which enhances the coupling of the unstable motion and the zonal field is the large axial scale ($8 \frac{\nu^{1/2}}{\Omega^{1/2}}$) of the disturbances.

Second, the long characteristic scale lengths of the disturbances

(22δ to 35δ) in an annulus of comparable radial scale would probably feel the constraint of curvature so that a given unstable wave should also be azimuthally periodic. The effect of curvature also enters into the R^{-1} dependence of the local Reynold's number, since the mean zonal velocity increases as R^{-1}; counter to this trend the maximum unstable waves predicted by Lilly's theory tend to move more slowly with respect to the zonal mean at higher Reynold's numbers; so it would be plausible that the most unstable waves across sizeable portions of the radius could have the same angular velocities.

5.4.2 The "Vorticity Jump"

We have seen that the maximum mean relative vorticity corresponds to the critical radius at which the non-steady Ekman layer develops instabilities. The oscillatory field in the core is coupled to the fluctuating Reynolds stresses in the transitional zones so that the viscous diffusion of the zonal fluctuations is effectively cancelled. The transitional zones in the mean appear to be non-divergent, since the mean circulations above them are constant. There are some exceptions which appear as small bumps in the circulation curves near the sink where a small net flux into the transitional layers is indicated. The change in vorticity which occurs across the transition zone is probably sufficient to form a very weak vertical shear layer. A few measurements were made in the core in these vorticity jump zones, but no oscillations distinguishable from other core waves were discernable.

5.4.3 Inertial Modes and the Observed Frequencies

In section 3.3 we found the relationships of the eigenvalues

for annular columns of fluid in solid body rotation. The perturbation frequency (n) is related to the vertical wave number (K) and the radial wave number (κ) by:

$$\kappa = \frac{K(4 - n^2)^{1/2}}{n}$$

The most energetic oscillations which we observed in the core of the annulus, had frequencies in the neighborhood of n~0.4 and ~0.86, where n is the non-dimensional frequency. In terms of inviscid oscillations of annulus is solid body rotation, these low frequencies would be associated with normal modes which have large radial wave numbers, as we noted in section 3. . Greenspan (1968, p. 83) had shown in the case of large $\kappa(m = 0)$ that the inertial modes of a cylinder in solid body rotation were altered by viscosity. Earlier Kudlick (1966, p. 75) had derived the explicit damping factors for these visco-inertial modes where $m \neq 0$ and $k \neq 0$; these analyses agree when a/H is large. The results obtained from the auto-and cross- correlations of the fluctuations at several radial positions indicate that the core waves do not have the high radial modes demanded by system in solid body rotation.

At this time we do not have the explicit solution for the perturbation problem for the annular core. It is probable that the observed frequencies may correspond to one of the normal modes of the vortex. The existence of Ekman layer-vortex resonances would further explain the sharp response of the core to the boundary layer waves. The core in resonance could act efficiently as a reservoir of information (fluctuating waves) which would force the Ekman layers to respond with coherency. The system would thus tend to "optimize" itself with respect

to the energy exchange between the boundary layers and the core. The amplitude spectra (Figures 6, 7A, and 8) are the electronically integrated output of the spectral analyzer, and the integration process tends to obscure the fact that all of the peaks below n = 1 have sharp cut-offs at the peak frequencies, so that the slopes of the high frequency sides of most peaks (n<1) are simply a representation of the decay time of the integrator.

Exchange of energies between the core and the boundary layers can also be interpreted in terms of the group velocities of the disturbances. Oser (1957) demonstrated that energy is propagated at an angle $\theta = \sin^{-1}(\frac{\sigma}{2\Omega})$ to the axis of rotation, thus a disturbance has group velocity whose vector resultant makes an angle θ with respect to the axis. The low frequencies of the boundary layer disturbances ($\frac{\sigma}{2\Omega} < 1$) which we observed are capable of exchanging energy with the core rather efficiently by slight distortions of the local vorticity field.

5.5 A Brief Summary

We can now see clearly that the unstable Ekman layers in our source-sink flow cannot be separated from the other types of motions within the system. Disturbances in the boundary layers propagate into the inviscid zonal flow, exciting larger scale oscillations throughout the core. In regions where the Ekman layers are laminar the core waves are damped by viscous diffusion and as a result there is an efflux of mass; this efflux is balanced by an increase of mean vorticity in the core. the transitional Ekman layers interact with the zonal flow through fluc-

tuating Reynold's stresses so that the viscous dissipation indirectly feeds the energy to the disturbance through the axial component of the zonal shear. The transitional boundary layers are, therefore, considered non-divergent in the mean, since they usually do not alter the mean vorticity of that portion of core which they bound.

Curvature of the flow appears to play an important part in the determination of the spatial scales of the instabilities in our apparatus, also the radial dependence of Reynold's number may tend to alter the instabilities.

The core and the Ekman layers have the same sharp and well-defined frequency spectra which indicates that there is a feedback response between the two types of motion; it is possible that the boundary layers establish a weak resonance with the core vortex. Figure 14 is a schematic of the basic exchanges in the flow.

The source and sink layer appear to be passive with respect to oscillations in the core and the Ekman layers; however at high flux the source layer does exhibit weak oscillatory motions which are probably responses to the more energetic interior waves.

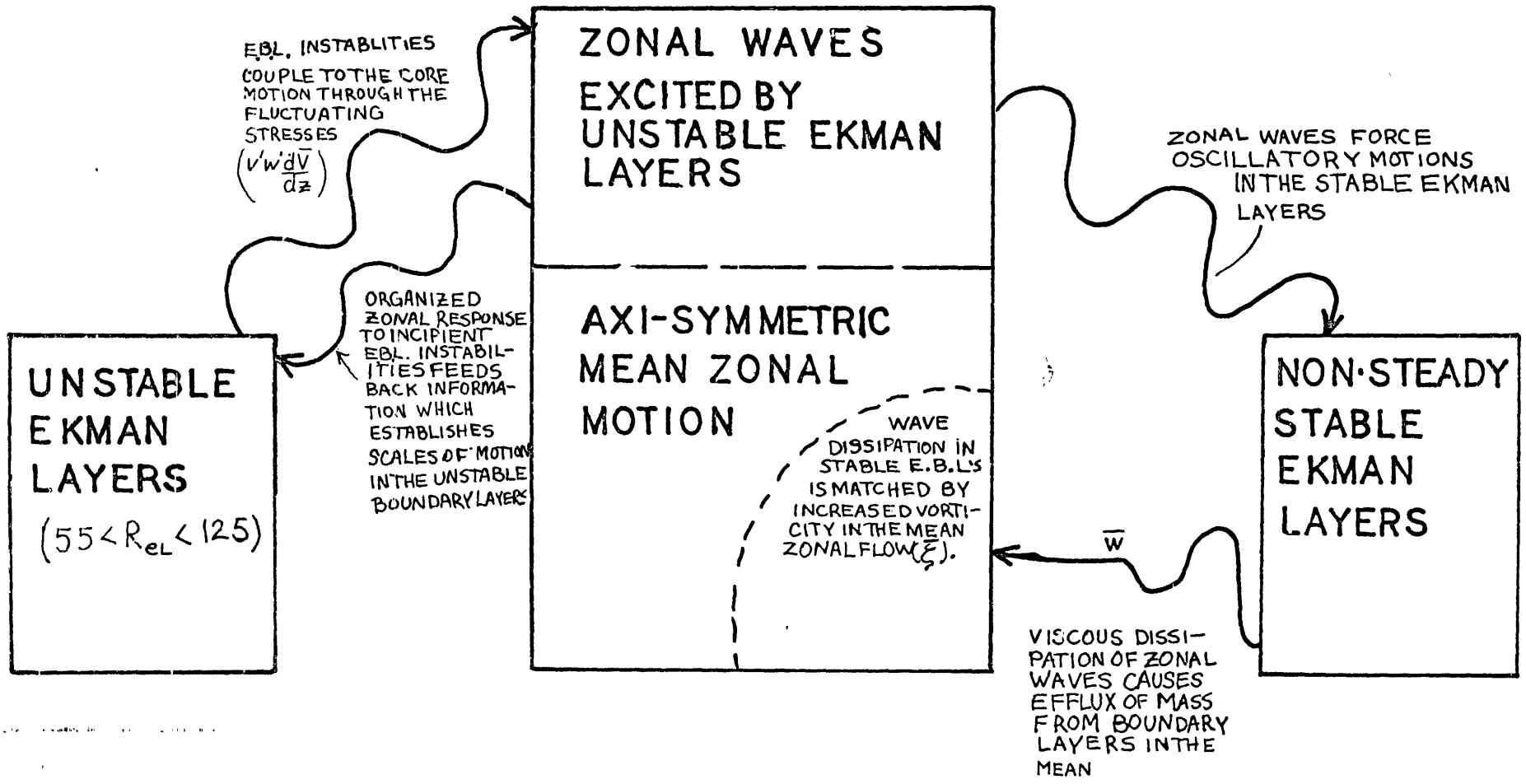

A schematic model of the Ekman Layer - Vortex interactions.

FIGURE 14

6.0 Possible Geophysical Implications

In our simple, highly controlled model we find that coupling of non-steady motions between the quasi-geostrophic core and the Ekman layers leads to states in which both Ekman layers and the zonal flow are altered. Also the classic spiral skewed shear profile of the steady Ekman layer was not observed in the mean. Scientists for years have used the conceptual artifice of the linear Ekman layer to understand the mean general oceanic and atmospheric circulation, even though they have seldom observed the ideal form of this boundary layer phenomenon in nature. The results of this experiment imply that the non-steady coupling between the boundary layers and the fluctuating zonal components must be taken into account in order to gain a more complete picture of the total role of the "real" Ekman layers in oceanic and atmospheric systems. One example, where the non-steady coupling could be important, would be in hurricanes. Oscillations of the boundary layer near the eye of the storm could force low frequency motions above the boundary layer. These inertial oscillations could then force motions in the more stable boundary layer at the outer edge of the storm. The forced response of the stable layer could result in an efflux of mass which would increase the vorticity (intensify) the storm.

Bibliography

Bjerknes, V., Bjerknes, J., Solberg, H., and Bergeron, T. (1933). Physicalische Hydrodynamik, Chapter II, Springer, Berlin.

Chandrasekhar, S. (1961). Hydrodynamic and Hydromagnetic Stability, 272-292.

Faller, A. (1963). "An experimental study of the instability of the laminar Ekman boundary layer." J. Fluid Mech., 15, 560-76.

Fultz, D. (1959). "A note on overstability and the elastoid-inertia oscillations of Kelvin, Solberg, and Bjerknes." Jour. of Meteorology, 16, 199-208.

Greenspan, H. (1968). The Theory of Rotating Fluids, the University Press, Cambridge.

Hide, R. (1968). "On source-sink flows in a rotating fluid." J. Fluid Mech., 32, 737-64.

Kelvin, Lord (1867). "Vortex Atoms." Proc. Roy. Soc. Edinb. Feb. 18.

Kelvin, Lord (1880). "Vibrations of a Columnar Vortex". Proc. Roy. Soc. Edinb., March 1.

Kudlick, M. (1966). "On the transient motions in a contained rotating fluid", Ph. D. thesis, Math. Dept., M.I.T.

Lewellen, W. (1965). "Linearized Vortex Flows." A.I.A.A. Journ., 3, 91-8.

Lilly, D. (1966). "Instability of Ekman boundary flow." Journ. Atm. Sciences, 23, 481-94.

Mollo-Christensen, E., Tatro, P., and Green, A. (1967). "Experiments on the stability and transition in an Ekman layer". presented at the I.U.G.G. and I.U.T.A.M. Symposium L966 in Kyoto. (Abstract in Physics of Fluids Suppl., 1967)

Oser, H. (1957). "Erzwungene Schwingungen in rotierenden Flusskeiten." Arch. Ratl. Mech. Anal., I, 81-96.

Phillips, O. (1960). "Centrifugal waves." J. Fluid Mech., 7, 340-52.

Rayliegh, Lord (1920). "On the dynamics of revolving fluids." Scientific Papers, 6, 447-53. Cambridge Univ. Press.

Roshko, A. (1954). "On the development of turbulent wakes from vortex streets." NACA TR 1191.

Tatro, P. (1966). "Experiments on Ekman layer instability." Ph.D. Thesis Depart. of Meteorology, M.I.T.

Tatro, P. and Mollo-Christensen, E. (1967). "Experiments on Ekman Layer Instability." J. Fluid Mech., 28, 531-44.

Appendix A

Velocity Sensors: Positioning and Calibration

A.1 Positioning

The mechanisms for hot wire positioning are featured in plates A1 and A2. Plate A1 shows that the hot wire axial and angle traversing mechanisms are mounted on two off-center circular discs which are imbedded in the upper plate of the annulus flush with its inner boundary. We shall refer to these disc inserts as the traversing plates. By rotating the traversing plates differentially the relative positions of the two sensors can be changed. The geometry of this configuration allows a sensor to traverse the radial extent of the annulus from about 1 cm. from the sink to 4 cm. from the outer wall; however, space and geometry limit the range of relative positions for both sensors.

Two means of determining radial positions of the sensors were tried during the course of the experiment. At first a triangulation of the sensor position was used; this required measurements of distances and angles from precisely known radii to the sensor. This procedure was very time consuming and was found to be only slightly more accurate than the direct measurements from the axis of the annulus to the sensor which varied only ± 1.5 mm. from the triangulations. As a means of standardizing the radial positions in the profile measurements of zonal velocities, index marks were made on the annulus and the traversing plates corresponding to each radial position of the sensor. Visual alignment of the index marks for a given position provided very good repeatability and simplicity.

Each change of radial or azimuthal position of the sensor also changes the orientation of the hot wire element to the flow in the interior of the apparatus. Corrections must be made each time the position is changed. The rough realignment is accomplished by visual alignment of the hot wire with the annulus axis. During calibration a small rod is set parallel to the hot wire element on the upper part of the sensor stem; the rod on the stem is aligned radially with the annulus. When the mean state is established in the rotating system the final orientation of the wire to the flow is made by maximizing the sensed mean velocity. This procedure requires use of the angle orientation mechanism.

The orientations of the hot wire elements in the rotating system are controlled by the small electric motors and gear drives at the tops of the axial traversing mechanisms in plate A-2 from a control panel in the laboratory. When measurements of the mean zonal component are desired, the maximization mentioned in the previous paragraph is accomplished by rotating the sensor until the voltage sensed across the hot wire element is minimized; this corresponds to the maximum mean zonal velocity.

Axial positions of the sensors are controlled by a worm gear, drives and screws. The gears are driven by the small electric motors at the bases of the traversing mechanisms. The worm gears turn the screws which are threaded through collars in the upper plates. Rotations of the screws move the tops of the mechanisms up and down along the smooth vertical rods mounted in the bottom plates. The sensors which are

affixed to the top parts of the mechanisms follow their motions. The change of axial positions is registered in the laboratory frame by electrical pulses from a six-lobed cam switch affixed to the end of the worm drive. Forty turns of the worm gear are required to advance the screw through one revolution, which moves the sensor axially 0.079cm. Each revolution of the worm causes six pulses to be sent to a counter on the position control panel; therefore, there are approximately 3030 pulses counted for each centimeter advanced by the sensor. The accuracy of this system was checked against a standard spring micrometer gauge and was found to agree within ±0.003 cm. The exact positions of the sensors relative to the axial boundaries could not be ascertained with the same accuracy, since there are unpredicable responses of the hot wire elements to the highly conductive metalic surfaces which form the boundaries, particularly at the low velocities encountered here. The "zero" positions were found in several cases when the sensor was unexpectedly forced into the boundary. The harbingers of these catastrophic collisions were sharp drops in sensor voltage, which are indications that the heat transfer process from the hot wire changes from force advection by the fluid to a mode of conduction to the boundary and the fluid in the viscous sublayer. This was observed to occur when the hot wire was 0.005 cm to 0.015 cm away from the boundary; thus we have a maximum uncertainty of approximately 0.02 cm in boundary layer thicknesses as we noted in section 4.

A.2 Calibration

Normally hot wire anemometers have been employed at considerably higher mean velocities in air than those which we measured in the annulus,

since most applications were in the field of aeronautics. In mean velocity fields ranging from near 0 cm/sec to 100 cm/sec we found that our hot wires, particularly in the x-arrays, did not respond to the flow in the "normal" ways, i.e., the over heat ratios of the hot wires did not follow the 1/2 power laws of velocity. There are two basic reasons for these deviations:

1. At low velocities ($\bar{V}$<20 cm/sec) the forced advection of heat from the hot wire is combined with the effect of gravitational convection. The total of these two types of heat transfer give an indication at the potentiometer that the ambient velocity is greater than the actual value. (For a detailed discussion of this see Collis and Chapman (1959). J. Fluid Mech, 6, p. 357.)
2. X-arrays of hot wires consists of two hot wire sensors perpendicular to each other at close proximity (~ 0.05cm). At low velocities the two wires heat the slow moving air around them enough so that they may interfere with each other and cause anomalous behavior of the sensor response to the mean flow and their angular orientations to it.

X-array sensors were employed throughout this experiment. At first they were used with the hope of measuring the radial component of the zonal flow, but it was found virtually impossible to calibrate and position the sensors accurately enough to make definitive measurements of the cross zonal components. Later as a point of consistency in measuring techniques the x-array was still used for the mean zonal velocity measurements. Measurements of the fluctuations in the flow were

made with single hot wire sensors.

The calibration of x-arrays is much more tedious than single hot wire arrays, since both wires in the x-array must be calibrated against a known velocity field at several angle orientations, but the general procedure is the same. Here we placed the sensors in a modified version of the wind tunnel used by Tatro (1966) in his thesis. The calibration velocities were found by counting the shedding frequencies from various small cylindrical bars extended across the working section of the tunnel. An empirical relation was used to determine the mean velocities from the shedding frequencies:

$$f = \frac{1}{d}\left(0.212\ U_o - \frac{4.5\nu}{d}\right)$$

where: f - shedding frequency

d - rod diameter

U_o - mean stream velocity

ν - kinematic viscosity

The voltage response across the hot wires was used to determine an over heat ratio (H).

$$H = \frac{IV_w}{V_w - IR_o}$$

where: V_w - voltage across the hot wire sensor

I - current through the hot wire

R_o - the ambient resistence of the unheated wire

The overheat ratio H is related to the mean steam velocity $\bar{V}$ by a power law: $H \propto BV^n$, where B is a coefficient peculiar to a given wire or array; normally for single wires $n \approx 1/2$. X-array varys considerably from

the $n \approx 1/2$ law, particularly at $\overline{V}<20$ cm/sec. The calibrations and determinations of the power law for x-arrays consisted of at least five sets of velocity-voltage pairs for each wire taken at various intervals of velocity from 12 cm/sec to 150 cm/sec. The power factor (n) is determined by taking a least squares fit of the relation:

$$\ln H = \ln B + n \ln \overline{V}$$

where the ambient temperature is constant. Changes in ambient temperature can alter the calibration values obtained from one time to another. When possible in this experiment mean velocity measurements were carried out over a narrow range of temperature.

Comparisons were made among various single and double hot wire sensors in order to determine a crude variance in sensed velocities. Single wire and x-arrays agreed well to less than 5% difference below 100 cm/sec; however at velocities over 150 cm/sec the difference grew to about 8%. The variances among sensors of the same types was usually less than 2%.

The divergence in indicated velocities between the two types of sensors is due to the insufficiency of a simple power law relation between overheat ratio and velocity for the x-array sensors over a wide range.

Appendix B

B.0 The Apparatus

B.1 Tolerances on Physical Dimensions

In this experiment it is essential that the annulus is axisymmetric with its rotation axis, otherwise periodic pressure fluctuations will occur in the system. The upper and lower disks which are the axial boundaries of the annulus were cut from flat sheets of aluminum jig plate 1/2" inch thick by a vertical lathe. The outer rims are concentric with respect to the hollow steel cylinder which separates them. The tolerances on the concentricity is $\pm$ 0.005 inches. The whole annulus assembly is mounted on a flange at the top of the hollow shaft on which the entire system rotates. The axes of the shaft and the annulus were aligned to within one milliradian using a high precision machinist's level.

During machining of the aluminum plates some stress relief warping occurred. Four adjustable spacers have been placed around the outer rims so that the plates could be made parallel ($\pm$ 0.020"). Even though the plates are essentially parallel, they are not perfectly flat, so that a waviness measurable in vertical displacements at the outer rim has a peak to peak amplitude of about 0.05 inches.

B.2 Source Walls

The outer vertical wall is both a boundary and a source for the fluid which moves through the system. Two types of construction using the same materials were tried. The first consisted of two sheets 1/4 inch thick reticulated polyurethane plastic foam which were separated by a one inch thick spacer. A band of paper was connected to the outside wall

of the inner sheet of foam midway between the upper and lower disks of the annulus. The paper covered all of the sheet except for two 3 cm. rings around the top and bottom of the annulus.

The second source wall consists of a single 1 inch thick section of the same type of plastic foam, and the whole area acts as a source. Numerous spot checks of mean zonal velocities and core oscillation frequencies taken over the operation range of the experiment were the same as the other source configuration.

Appendix C

B.0 Flux Control

B.1 Calibration

The low volume flux from source to sink is particularly difficult to measure by the standard methods which rely on measurment of pressure gradients. Here the flow meter which is used to measure the net flux consists of a 4.5 cm brass tube; three thin layers of reticulated foam inserted in this tube across the flow at intervals of about one centimeter. About three centimeters downstream of the last section of foam, a 0.182 cm cylinder is installed perpendicular to the flow. When the velocity of the flow through the meter exceeds 600 cc/sec. a regular von Karman vortex street forms in the wake of the cylinder. The frequency at which the eddies in the vortex street move past a point slightly abaft the cylinder is proportional to the mean stream velocity; the frequency is also proportional to the volume flux through the tube, since the flux is directly proportional to the velocity. The relation between volume flux and shedding frequency is obtained by measuring frequency of voltage fluctuations registered by a hot wire anemometer placed in the vortex street and comparing this with the volume flux indicated by an American Meter Corporation bell-type prover (10 cu. ft.). The prover is purported to be accurate within 1/2% of the actual volume flux.

Table C-1 is the result of the frequency versus volume flux calibration from the flow meter and the prover. The relation of frequency to flux as measured is very nearly linear, but it does not correspond to

the result one would obtain by simply computing the volume flux from the cross sectional area and the shedding frequency formula by Roshko (1954) noted in appendix A:

$$S = \pi r_o^2 [4.72d(f + 4.5)] \tag{C.1}$$

where f and d are defined as in appendix A and r_o is the radius of the flow meter. This simple relationship is more accurate than one which takes the effective thickness of the side wall boundary layer on the tube into account:

$$S = \pi[r_o\sqrt{4.72d}\ (f + \frac{4.5\nu}{d})^{1/2} - 1.72\sqrt{x\nu}] \tag{C.2}$$

where $1.72\sqrt{x\nu}$ is the displacement thickness of the boundary layer.

The empirical relation was found to be:

$$S(\frac{cm^3}{sec}) = 220(\pm 5) + (14 \pm .1)f \tag{C.3}$$

formula (C.1) would give

$$S(\frac{cm^3}{sec}) = 288 + 13.6f \tag{C.4}$$

B.2 Control

Long term flux control within the narrow limits necessary here is difficult because of the inherent speed instability of ordinary fans or blower systems. High frequency noises can propagate upstream from the whirling blades as pressure pulses. Also the air ducting may have preferred frequencies which may resonate with the fluctuations in the flow. The baffle, perforated cylindrical sleeve and the constant speed axial fan (Figure 4) were found sufficient to overcome these problems.

The fan works against a constant pressure head determined by the amount of the perforated cylinder which is covered. The perforations allow the air, which passes through them, to enter the system uniformly so that no "chuffing" occurs due to irregular motions.

Table C-1

Measured Volume Flux (S) $cm^3 sec^{-1}$	Frequency (f) sec^{-1}
669	33
807	44
991	56
1123	66
1773	116
2256	150
3236	215

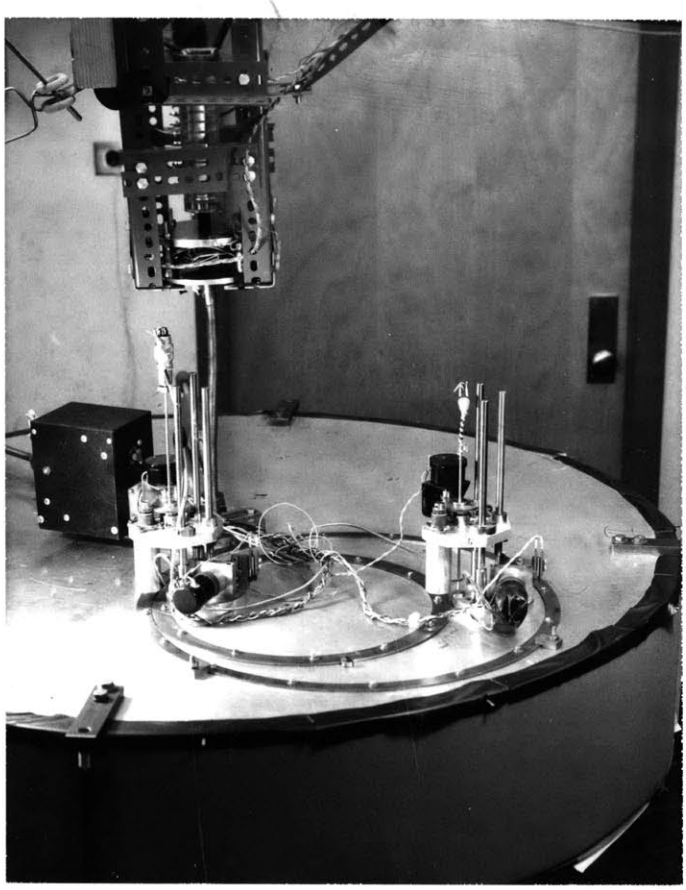

Plate A-1. Velocity sensor position control.

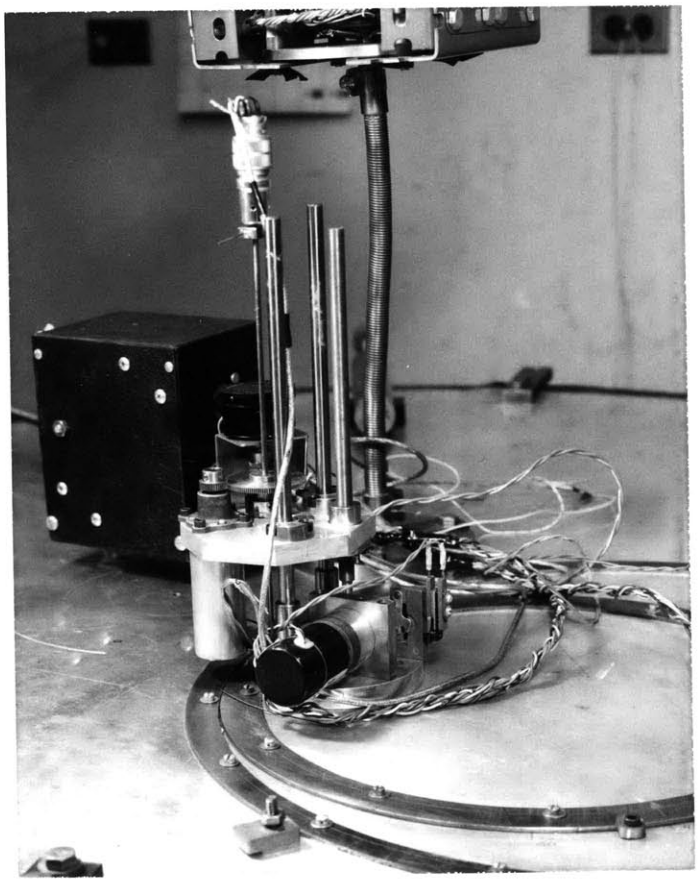

Plate A-2. Detail of the axial traversing mechanism.

List of Symbols

α = a large number

$\beta = (\frac{2+n}{2-n})$

$\Gamma = \frac{VR}{\Omega \bar{a}}$ - non-dimensional circulation in rotating frame.

Δ = non-dimensional radial displacement

$\bar{\delta}$ = average boundary layer thickness (observed) $\sim 1.7(\nu/\Omega)^{1/2}$

δ_1 = observed thickness of zonal shear in boundary layer

$\delta_2 = \frac{4z}{\pi}$ - the thickness of the Ekman layer based on the observed distance (z) above the boundary where the maximum in the radial component in the layer occurs.

$\varepsilon = \bar{V}/\Omega aR$ = local Rossby number of the mean zonal flow.

$\bar{\xi}$ = mean axial component of the vorticity

η = z/H - non-dimensional axial position

θ = azimuthal (zonal) angle

κ = radial eigenvalue for inertial modes

ν = kinematic viscosity

Ξ = non-dimensional pressure perturbation

ρ = fluid density

Σ = non-dimensional perturbation pressure

τ (Ωt) - non-dimensional time also used as non-dimensional delay time in correlations

$\Phi = 2(1+\varepsilon)[2(1+\varepsilon) - D\varepsilon]$ - Rayliegh discriminant for stability

χ = non-dimensional zonal perturbation velocity

ψ = radial perturbation velocity

Ω = rotation rate

A = a non-dimensional proportionlity factor

a - the radius of the annulus at source wall

b - the non-dimensional radius of the sink wall

d - characteristic Ekman thickness $(\nu/\Omega)^{1/2}$

E - Ekman number $(\nu/\Omega H^2)$

$E'/E_{r.m.s.}$ - voltage fluctuations at sensor normalized against the r.m.s. of these fluctuations.

f - shedding frequency of a rod

H - height of the annulus

$\vec{K}$ - axial unit vector

κ - axial wave number (non-dimensional) = $\frac{q2\pi a}{H}$, (q = 1, 2, 3...)

m - zonal wave number

n - non-dimensioal frequency of the perturbation

p - pressure

$\bar{p}$ - mean ambient pressure

p' - non-steady pressure fluctuations

R - non-dimensional radius = r/a

S - volume flux rate

T - period of rotation

t - time also(τ') in the real time delays in correlations
u - vector tatal velocity in the inviscid core
u - radial velocity component
V'- fluctuations of the zonal component
$\overline{V}$ - mean zonal compoent
W - axial velocity component
$\overline{W}$ - mean axial velocity above E.B.L.
$R_{AA}(0)$, $R_{BB}(0)$ - mean square of voltage fluctuations at sensor channels A and B.
$R_{AA}(\tau)$, $R_{BB}(\tau)$ - auto correlation functions of fluctuations with τ as the variable time delay.
$R_{AB}(\tau)$ - cross correlation function of observed fluctuations of sensor voltage.
R_{reL} - $\overline{V}\delta/\nu$ - local Reynold's number
R_{OL} - $\overline{V}/\Omega aR$ - local Rossby number
R_{OS} - $\overline{V}/\Omega a$ - system Rossby number

Biography

The author was born December 15, 1938 in Jackson, Mississippi and he received his early education in the public schools and at Mississippi College in Clinton. In 1956 he entered Vanderbilt University where he received a Batchelor of Arts degree in Physics in 1960. Upon graduation he entered the naval service. In the navy he was assigned as technical supervisor for preflight testing of guided missiles and telemetry of Talos missiles during the later part of their operational evaluation on the USS Galveston. Shortly after completion of naval service he received a trainee fellowship in health physics from the U.S. A.E.C. Soon after completion of this fellowship in August 1964, he enrolled in M.I.T. in the Department of Meteorology.